Extended-soft-core Baryon-Baryon ESC16 model IV. $S = -3, -4$ Hyperon-hyperon Interactions

M.M. Nagels
Institute of Mathematics, Astrophysics, and Particle Physics
University of Nijmegen, The Netherlands

Th.A. Rijken*
Institute of Mathematics, Astrophysics, and Particle Physics
University of Nijmegen, The Netherlands and
Nishina Center for Accelerator-Based Science, Institute for Physical and Chemical Research (RIKEN). Wako, Saitama, 351-0198, Japan

Y. Yamamoto†
Nishina Center for Accelerator-Based Science, Institute for Physical and Chemical Research (RIKEN). Wako, Saitama, 351-0198, Japan
(Dated: version of: May 27, 2022)

Background: This paper presents the Extended-Soft-Core (ESC) potentials ESC16 for baryon-baryon (BB) channels with total strangeness $S = -3, -4$. For these channels no experimental scattering data exist, and also there is no information from hypernuclei or hyperonic matter.

Purpose: The aim is to calculate the predictions of the ESC16 model for the $S = -3, -4$ BB channels.

Methods: The potential models for $S = -3, -4$ are based on SU(3) extensions of potential models for the $S = 0, -1$ and $S = -2$ sectors, which are fitted to experimental data. Flavor SU(3)-symmetry is broken 'kinematically' by the masses of the baryons and the mesons. The fit to the $S = 0, -1$ sectors provides the necessary constraints to fix all free parameters, *i.e.* baryon-baryon-meson (BBM) couplings and cut-off masses. The $S = -2$ systems are constrained by the $\Delta B_{\Lambda\Lambda}$ value from the Nagara event, and the requirement of $U_\Xi \approx -10$ MeV.

Resuls: Various properties of the potentials are illustrated by giving results for scattering lengths, bound states, phase-parameters, and total cross sections.

Conclusions: No BB bound states have been predicted by the ESC16 model.

PACS numbers: 13.75.Ev, 12.39.Pn, 21.30.-x

I. INTRODUCTION

In this paper we present the results of the ESC16-model for channels with total strangeness $S = -3, -4$ channels. This is further SU(3) generalization of the ESC16 companion models on NN [1], YN [2], and YY [3] for baryon-baryon channels with, henceforth referred to as paper I, II, and III respectively. In this paper the Extended-Soft-Core (ESC) potentials ESC16, described in the companion nucleon-nucleon (NN) [1] and the hyperon-nucleon/hyperon (YN,YY) papers [2, 3] for baryon-baryon channels with $S = 0, -1, -2$. These papers will be referred to as paper I, II, and III respectively. A Similar approach has been performed in [12], where the Nijmegen soft-core one-boson-exchange (OBE) interactions NSC97a-f for baryon-baryon (BB) systems for $S = -2, -3, -4$ were presented.

For the $S = -3, -4$ channels no experimental scattering information is available, and also the information from hypernuclei is non-existent. For $S = -2$ there are data on double $\Lambda\Lambda$-hypernuclei, which recently became very much improved by the observation of the Nagara-event [13]. This event indicates that the $\Lambda\Lambda$-interaction is rather weak, in contrast to the estimates based on the older experimental observations [14, 15]. This has always been a characteristic feature of the Nijmegen soft-core models. The ESC16 model describes all experimental information on the $S = 0, -1, -2$ systems, two-body scattering and hypernuclei, very satisfactorily. Therefore, the predictions for $S = -3, -4$ may very well be realistic.

The study of strangeness-rich systems is of importance in understanding relativistic heavy-ion collisions [16], some astrophysical problems [17, 18], and the existence (or nonexistence) of certain hypernuclei. Strangeness-rich systems can be exotic multi-quark systems consisting of up (u), down (d), and strange (s) quarks; like the elusive H dibaryon, a 6-quark $uuddss$ system predicted by Jaffe [19]. But they can also simply be bound states of nucleons (N), hyperons ($Y = \Lambda, \Sigma$), and cascades (Ξ). In order to get a better handle on the latter possibility, we are in need of potential models which describe all possible interactions between nucleons, hyperons, and cascades.

In the absense of experimental information for S<-3,-4, we assume that the potentials obey (broken) flavor SU(3) symmetry. As in papers I-III, the $S = -3, -4$ potentials

*t.rijken@science.ru.nl
†ys_yamamoto@riken.jp

are parametrized in terms of meson-baryon-baryon, and meson-pair-baryon-baryon couplings and gaussian form factors. This enables us to include in the interaction one-boson-exchange (OBE), two-pseudoscalar-exchange (TME), and meson-pair-exchange (MPE), without any new parameters. All parameters have been fixed by a simultaneous fit to the NN and YN data, scattering and hypernuclear, see I and II. Each NN⊕YN-model leads to a YY-model in a well defined way. SU(3)-symmetry allows us to define all coupling constants needed to describe the multi-strange interactions in the baryon-baryon channels occurring in $\{8\}\otimes\{8\}$. In all ESC models it is assumed that the coupling constants, apart from meson-mixing, are SU(3)-symmetric. The succes of the ESC models for example, suggests that deviations from SU(3) symmetry are small.

Quantum-chromodynamics (QCD) is, as generally accepted now, the physical basis of the strong interactions. Since in QCD the gluons are flavor blind, SU(3)-symmetry is a basic symmetry, which is broken by the chiral-symmetry-breaking at low energies. This picture supports our assumptions, stated above, on SU(3)-symmetry. The coupling constants and the $F/(F+D)$-ratio's used in the ESC models follow the predictions of the $^3P_0$ $^{-3}$ S_1 quark-pair creation model (QPC) rather closely [1, 10], with the domination of the $^3P_0$-mechanism [20]. Now, it has been shown that in the strong-coupling Hamiltonian lattice formulation of QCD, the flux-tube model, that this is indeed the dominant picture in flux-tube breaking [21]. Therefore, since the ESC models are rather QCD-based, the predictions for the $S=-2,-3,-4$-channels are fairly realistic predictions. In III new phenomenological gaussian SU(3)-symmetric two-body BB potentials are introduced in addition to the meson- and meson-pair-exchanges to investigate the possible incompleteness of the ESC-interactions considered thus far in the ESC models. The motivation for this are the recent S=-2 hypernuclei experimental observations [4–6] and G-matrix calculations. Fitting to the NN⊕YN⊕YY data resulted in good BB well-depths. In this paper we include the $S=-3,-4$ results for the variant ESC16*(A) [3].

Most of the details on the SU(3) description are well known, and in particular for baryon-baryon scattering they can be found in papers I-III, and e.g. [12, 22, 23]. So, here we restrict ourselves to a minimal exposition of these matters, necessary for the readability of this paper. In Sec. II we first review for $S=-3,-4$ baryon-baryon thresholds and the multi-channel description. We repeat the SU(3)-symmetric interaction Lagrangian describing the interaction vertices between mesons and members of the $J^P=(1/2)^+$ baryon octet, and define their coupling constants. We then identify the various channels which occur in the $S=-3,-4$ baryon-baryon systems. We describe the R-conjugation operation which is useful for the comparison of the $(\Lambda\Xi,\Sigma\Xi)$- and the $\Lambda N,\Sigma N)$-potentials. In Appendix C the potentials on the isospin basis are given in terms of the SU(3)-irreps. In most cases, the interaction is a multi-channel interaction, characterized by transition potentials and thresholds. Details were given in [12, 22]. For the details on the pair-interactions, we refer to Ref. [11]. In Sec. IV we describe briefly the treatment of the multi-channel thresholds in the potentials. In Sec. VI we present the results of the ESC16 potentials for all the sectors with total strangeness $S=-3,-4$. We give the couplings and $F/(F+D)$-ratio's for OBE-exchanges of ESC16 . Similarly, tables with the pair-couplings are shown in Appendix A. We give the S-wave scattering lengths, discuss the possibility of bound states in these partial waves. Also, we give the S-matrix information for the elastic channels in terms of the Bryan-Klarsfeld-Sprung (BKS) phase parameters [24–26], or in the Kabir-Kermode (KK) [27] format. Tables with the BKS-phase parameters are displayed in Appendix B. Such information is very usefull for example for the construction of the Λ-, Σ-, and Ξ-nucleus potentials. We also give results for the total cross sections for all leading channels.

We conclude the paper with a summary and some final remarks in Sec. VII.

II. CHANNELS, POTENTIALS, AND SU(3) SYMMETRY

A. Multi-channel Formalism

For the kinematics and the definition of the amplitudes, we refer to paper II of this series. Similar material can be found in [23]. Also, in paper I the derivation of the Lippmann-Schwinger equation in the context of the relativistic two-body equation is described.

On the physical particle basis, there are four charge channels:

$$\begin{aligned}
q=+1: &\quad \Sigma^+\Xi^0\to\Sigma^+\Xi^0,\\
q=\ \ 0: &\quad (\Lambda\Xi^0,\Sigma^0\Xi^0)\to(\Lambda\Xi^0,\Sigma^0\Xi^0)\ ;\ \Xi^0\Xi^0\to\Xi^0\Xi^0,\\
q=-1: &\quad (\Lambda\Xi^-,\Sigma^0\Xi^-,\Sigma^-\Xi^0)\to(\Lambda\Xi^-,\Sigma^0\Xi^-,\Sigma^-\Xi^0)\ ;\ \Xi^0\Xi^-\to\Xi^0\Xi^-,\\
q=-2: &\quad \Sigma^-\Xi^-\to\Sigma^-\Xi^-\ ;\ \Xi^-\Xi^-\to\Xi^-\Xi^-.
\end{aligned}\tag{2.1}$$

We note here that in strong interactions S is conserved and hence in the q=-1,-2 channels there is no coupling of the ΞΞ-channelis in (2.1) with the others.

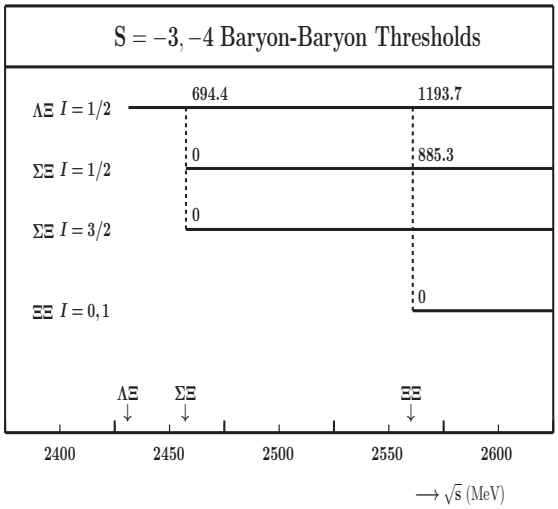

FIG. 1: Thresholds in YY-channels for $S = -3, -4$.

Like in [22, 23], the potentials are calculated on the isospin basis. For $S = -3, -4$ hyperon-hyperon systems there are three isospin channels:

$$\begin{aligned} Y = -1, S = -3, I = 1/2: &\quad (\Lambda\Xi, \Sigma\Xi \to \Lambda\Xi, \Sigma\Xi), \\ Y = -1, S = -3, I = 3/2: &\quad (\Sigma\Xi \to \Sigma\Xi), \\ Y = -2, S = -4, I = 0, 1: &\quad (\Xi\Xi \to \Xi\Xi). \end{aligned} \tag{2.2}$$

The relation between the charge, isospin and hypercharge is given by the Gell-Mann-Nishijima relation $Q = Y/2 + I_3$, where in terms of the baryon number (B) and strangeness (S) the hypercharge Y=B+S.

The two-particle thresholds in the YY-channels for S=-3,-4 are shown in Fig. 1. The relation between the isospin and charge is given by the Gell-Mann-Nishijima relation $Q = Y/2 + I_3$, where the hypercharge Y=B+S.

For the kinematics of the reactions and the various thresholds, see [22]. In this work we do not solve the Lippmann-Schwinger equation, but the multi-channel Schrödinger equation in configuration space, completely analogous to [23]. The multi-channel Schrödinger equation for the configuration-space potential is derived from the Lippmann-Schwinger equation through the standard Fourier transform, and the equation for the radial wave function is found to be of the form [23]

$$u''_{l,j} + (p_i^2 \delta_{i,j} - A_{i,j}) u_{l,j} - B_{i,j} u'_{l,j} = 0, \tag{2.3}$$

where $A_{i,j}$ contains the potential, nonlocal contributions, and the centrifugal barrier, while $B_{i,j}$ is only present when non-local contributions are included. The solution in the presence of open and closed channels is given, for example, in Ref. [28]. The inclusion of the Coulomb interaction in the configuration-space equation is well known and included in the evaluation of the scattering matrix.

Obviously, the potentials on the particle basis for the $Y = -2$ channels are given by the $I = 0, 1$ $\Xi\Xi$-potential on the isospin basis. For $Y = -1$ channels the potentials are related to the potentials on the isospin basis by an isospin rotation. Ordering the channels in the $q = 0$ sector according to increasing rest mass $(\Lambda\Xi^0, \Sigma^0\Xi^0, \Sigma^+\Xi^-)$ one obtains in channel space the potential matrix , $V_{ab}(I) \equiv V_{a,\Xi;b,\Xi}(I)$, with $a, b \equiv \Lambda, \Sigma$,

$$V(q = 0, Y = -1) = \begin{pmatrix} V_{\Lambda\Lambda}(\frac{1}{2}) & -\sqrt{\frac{1}{3}} V_{\Lambda\Sigma} & \sqrt{\frac{2}{3}} V_{\Lambda\Sigma} \\ -\sqrt{\frac{1}{3}} V_{\Lambda\Sigma} & \frac{1}{3}\left[V_{\Sigma\Sigma}(\frac{1}{2}) + 2V_{\Sigma\Sigma}(\frac{3}{2})\right] & \frac{\sqrt{2}}{3}\left[-V_{\Sigma\Sigma}(\frac{1}{2}) + V_{\Sigma\Sigma}(\frac{3}{2})\right] \\ \sqrt{\frac{2}{3}} V_{\Lambda\Sigma} & \frac{\sqrt{2}}{3}\left[-V_{\Sigma\Sigma}(\frac{1}{2}) + V_{\Sigma\Sigma}(\frac{3}{2})\right] & \frac{1}{3}\left[2V_{\Sigma\Sigma}(\frac{1}{2}) + V_{\Sigma\Sigma}(\frac{3}{2})\right] \end{pmatrix}, \tag{2.4}$$

and for $q=-1$ we have now the ordering $(\Lambda\Xi^-, \Sigma^-\Xi^0, \Sigma^0\Xi^-)$, and we get for the potential matrix

$$V(q=-1,Y=-1)=\begin{pmatrix} V_{\Lambda\Lambda}(\frac{1}{2}) & -\sqrt{\frac{2}{3}}V_{\Lambda\Sigma} & \sqrt{\frac{1}{3}}V_{\Lambda\Sigma} \\ -\sqrt{\frac{2}{3}}V_{\Lambda\Sigma} & \frac{1}{3}\left[2V_{\Sigma\Sigma}(\frac{1}{2})+V_{\Sigma\Sigma}(\frac{3}{2})\right] & \frac{\sqrt{2}}{3}\left[-V_{\Sigma\Sigma}(\frac{1}{2})+V_{\Sigma\Sigma}(\frac{3}{2})\right] \\ \sqrt{\frac{1}{3}}V_{\Lambda\Sigma} & \frac{\sqrt{2}}{3}\left[-V_{\Sigma\Sigma}(\frac{1}{2})+V_{\Sigma\Sigma}(\frac{3}{2})\right] & \frac{1}{3}\left[V_{\Sigma\Sigma}(\frac{1}{2})+2V_{\Sigma\Sigma}(\frac{3}{2})\right] \end{pmatrix}, \tag{2.5}$$

The connection between the BB isospin states and the SU(3)-irreps is given in Table I, and in the figures of Appendix A the NN, YN, and YY content is given for the irreps {8}, {27}, {10*}, and {10}.

The momentum space and configuration space potentials for the ESC16-model have been described in paper I and II for baryon-baryon in general. Therefore, they apply also to hyperon-nucleon and we can refer for that part of the potential to paper I. Also in the ESC-model, the potentials are of such a form that they are exactly equivalent in both momentum space and configuration space. The treatment of the mass differences among the baryons are handled exactly similar as is done in [22, 23]. Also, exchange potentials related to strange meson exchange K, K^* etc. , can be found in these references.

The baryon mass differences in the intermediate states for TME- and MPE- potentials has been neglected for *YN*-scattering. This, although possible in principle, becomes rather laborious and is not expected to change the characteristics of the baryon-baryon potentials.

TABLE I: SU(3) content of the different interaction channels. S is the total strangeness and I is the isospin. The upper half refers to the space-spin symmetric states $^3S_1$, $^1P_1$, ^3D, ..., while the lower half refers to the space-spin antisymmetric states $^1S_0$, ^3P, $^1D_2$, ...

Space-spin symmetric			
S	I	Channels	SU(3)-irreps
0	0	NN	$\{10^*\}$
–1	1/2	ΛN, ΣN	$\{10^*\}$, $\{8\}_a$
	3/2	ΣN	$\{10\}$
–2	0	ΞN	$\{8\}_a$
	1	ΞN, $\Sigma\Sigma$	$\{10\}$, $\{10^*\}$, $\{8\}_a$
		$\Sigma\Lambda$	$\{10\}$, $\{10^*\}$
–3	1/2	$\Xi\Lambda$, $\Xi\Sigma$	$\{10\}$, $\{8\}_s$
	3/2	$\Xi\Sigma$	$\{10^*\}$
–4	0	$\Xi\Xi$	$\{10\}$
Space-spin antisymmetric			
S	I	Channels	SU(3)-irreps
0	1	NN	$\{27\}$
–1	1/2	ΛN, ΣN	$\{27\}$, $\{8\}_s$
	3/2	ΣN	$\{27\}$
–2	0	$\Lambda\Lambda$, ΞN, $\Sigma\Sigma$	$\{27\}$, $\{8\}_s$, $\{1\}$
	1	ΞN, $\Sigma\Lambda$	$\{27\}$, $\{8\}_s$
	2	$\Sigma\Sigma$	$\{27\}$
–3	1/2	$\Xi\Lambda$, $\Xi\Sigma$	$\{27\}$, $\{8\}_s$
	3/2	$\Xi\Sigma$	$\{27\}$
–4	1	$\Xi\Xi$	$\{27\}$

B. SU(3) Symmetry and R-conjugation

The SU(3)-invariant interaction Hamiltonian for the baryon-baryon (BB) pseudoscalar meson interaction reads [30]

$$\begin{aligned}\mathcal{H}_I &= g_{P,8}\sqrt{2}\{\alpha_P\left[\bar{B}BP\right]_F+(1-\alpha_P)\left[\bar{B}BP\right]_D\} \\ &\quad +g_{P,1}\left[\bar{B}BP\right]_S. \end{aligned}\tag{2.6}$$

Here, the baryons are the members of the $J^P=\frac{1}{2}^+$ baryon octet

$$B=\begin{pmatrix} \frac{\Sigma^0}{\sqrt{2}}+\frac{\Lambda}{\sqrt{6}} & \Sigma^+ & p \\ \Sigma^- & -\frac{\Sigma^0}{\sqrt{2}}+\frac{\Lambda}{\sqrt{6}} & n \\ -\Xi^- & \Xi^0 & -\frac{2\Lambda}{\sqrt{6}} \end{pmatrix}. \tag{2.7}$$

The meson nonet 3×3 matrix P can be written as

$$P=P_{\{1\}}+P_{\{8\}}, \tag{2.8}$$

where the singlet 3×3 matrix $P_{\{1\}}$ has the elements $\eta_0/\sqrt{3}\delta^\alpha_\beta$, and the octet matrix $P_{\{8\}}$ is given by

$$P_{\{8\}}=\begin{pmatrix} \frac{\pi^0}{\sqrt{2}}+\frac{\eta_8}{\sqrt{6}} & \pi^+ & K^+ \\ \pi^- & -\frac{\pi^0}{\sqrt{2}}+\frac{\eta_8}{\sqrt{6}} & K^0 \\ K^- & \overline{K^0} & -\frac{2\eta_8}{\sqrt{6}} \end{pmatrix}. \tag{2.9}$$

Similarly the interaction with the vector $J^{PC}=1^{--}$, scalar $J^{PC}=0^{++}$, axial-vectors $J^{PC}=1^{++}$ and $J^{PC}=$

1^{+-} mesons. With the SU(2) isosinglet Λ, isodoublets

$$N = \begin{pmatrix} p \\ n \end{pmatrix}, \quad \Xi = \begin{pmatrix} \Xi^0 \\ \Xi^- \end{pmatrix}, \quad \text{and}$$
$$K = \begin{pmatrix} K^+ \\ K^0 \end{pmatrix}, \quad K_c = \begin{pmatrix} \overline{K^0} \\ -K^- \end{pmatrix}, \qquad (2.10)$$

and isovector $\Sigma^+, \Sigma^0, \Sigma^-$, the SU(3) invariant interaction Hamiltonian (2.6) can be written in the isospin basis, see *e.g.* [30] and [3] formula (2.9). All coupling constants can be expressed in terms of only four parameters. The explicit expressions can be found in Refs. [22, 30]. For example, in the case of the pseudoscalar mesons the parameters are (i) the octet coupling $g_{NN\pi}$, the F/(F+D)-ratio α_P, the singlet coupling g_{η_0}, and the $\eta_8 - \eta_0$ mixing angle θ_P.

In Table II the relation between the potentials on the isospin-basis is given, see (2.4)-(2.5), and the SU(3)-irreps. Here $V_{\Xi\Xi} = V_{\Xi\Xi,\Xi\Xi}, V_{\Lambda\Lambda} = V_{\Lambda\Xi,\Lambda\Xi}$ etc.

TABLE II: SU(3)$_f$-contents of the various potentials on the isospin basis.

Space-spin antisymmetric states $^1S_0,\ ^3P,\ ^1D_2, ...$	
$\Xi\Xi \to \Xi\Xi$ $Y=-2, I=1$	$V_{\Xi\Xi}(I=1) = V_{27}$
$\Lambda\Xi \to \Lambda\Xi$	$V_{\Lambda\Lambda}\left(I=\frac{1}{2}\right) = \left(9V_{27} + V_{8_s}\right)/10$
$\Lambda\Xi \to \Sigma\Xi$ $Y=-1, I=\frac{1}{2}$	$V_{\Sigma\Lambda}\left(I=\frac{1}{2}\right) = \left(-3V_{27} + 3V_{8_s}\right)/10$
$\Sigma\Xi \to \Sigma\Xi$	$V_{\Sigma\Sigma}\left(I=\frac{1}{2}\right) = \left(V_{27} + 9V_{8_s}\right)/10$
$\Sigma\Xi \to \Sigma\Xi$ $Y=-1, I=\frac{3}{2}$	$V_{\Sigma\Sigma}\left(I=\frac{3}{2}\right) = V_{27}$
Space-spin symmetric states $^3S_1,\ ^1P_1,\ ^3D, ...$	
$\Xi\Xi \to \Xi\Xi$ $Y=-2, I=0$	$V_{\Xi\Xi}(I=0) = V_{10}$
$\Lambda\Xi \to \Lambda\Xi$	$V_{\Lambda\Lambda}\ \left(I=\frac{1}{2}\right) = \left(V_{10} + V_{8_a}\right)/2$
$\Lambda\Xi \to \Sigma\Xi$ $Y=-1, I=\frac{1}{2}$	$V_{\Sigma\Lambda}\left(I=\frac{1}{2}\right) = \left(V_{10} - V_{8_a}\right)/2$
$\Sigma\Xi \to \Sigma\Xi$	$V_{\Sigma\Sigma}\left(I=\frac{1}{2}\right) = \left(V_{10} + V_{8_a}\right)/2$
$\Sigma\Xi \to \Sigma\Xi$ $Y=-1, I=\frac{3}{2}$	$V_{\Sigma\Sigma}\left(I=\frac{3}{2}\right) = V_{10^\star}$

To compare the SU(3)-structure for the BB-states Gell-Mann's R-conjugation [32, 33] is useful. R-conjugation is the inversion operation on the baryon and pseudo-scalar octet states

$$p \leftrightarrow \Xi^-, \quad n \leftrightarrow \Xi^0, \quad \Lambda \leftrightarrow \Lambda, \quad \Sigma^0 \leftrightarrow \Sigma^0, \qquad (2.11)$$
$$K^+ \leftrightarrow K^-, \quad K^0 \leftrightarrow \bar{K}^0, \quad \eta \leftrightarrow \eta, \quad \pi^0 \leftrightarrow \pi^0. \qquad (2.12)$$

For the BB-states one has

$$\begin{aligned} R\psi_{27}(Y,I,I_3) &= \psi_{27}(-Y,I,-I_3)\ , \\ R\psi_{10}(Y,I,I_3) &= \psi_{10^\star}(-Y,I,-I_3)\ , \\ R\psi_{8_s}(Y,I,I_3) &= \psi_{8_s}(-Y,I,-I_3)\ , \\ R\psi_{8_a}(Y,I,I_3) &= -\psi_{8_a}(-Y,I,-I_3)\ , \\ R\psi_1(Y,I,I_3) &= \psi_1(-Y,I,-I_3). \end{aligned} \qquad (2.13)$$

Therefore, in comparing the SU(3)-structure of the $(\Lambda N, \Sigma N)$-potentials with the $(\Lambda\Xi, \Sigma\Xi)$-potentials the irreps $\{10\}$ and $\{10^\star\}$ are interchanged. Similarly, for the NN-potentials and the $\Xi\Xi$-potentials. The entries of Table II, apart from using SU(3) Clebsch-Gordan coefficients, can be derived from Table I in Ref. [2] using R-conjugation.

The R-conjugation is not an SU(3)-transformation, and also it is not a symmetry of the strong-interactions. The latter would mean no $\{8_s\} \leftrightarrow \{8_a\}$-transitions, because $\langle\{8_a\}|V|\{8_s\}\rangle = \langle\{8_a\}|R^{-1}VR|\{8_s\}\rangle = -\langle\{8_a\}|V|\{8_s\}\rangle = 0$. This implies that the transitions $^1P_1 \leftrightarrow ^3P_1$ are forbidden, and so no anti-symmetric spin-orbit forces. However, for the vector- and axial-vector exchange with different F/(F+D) ratios for the direct and derivative couplings the antisymmetric spin-orbit potentials are non-zero, while having SU(3) symmetry. The potentials in an SU(3)-irrep have the form $V_{\{\mu\}} = g f_{\{\mu\}}(\alpha)$ where $f_{\{\mu\}}(\alpha)$. The extra restriction from R-conjugation symmetry w.r.t. SU(3) is that $f_{\{10\}}(\alpha) = f_{\{10^*\}}(\alpha)$. Then, the central-, spin-spin-, tensor-, spin-orbit-, and quadratic spin-orbit potential have R-symmetry for exact SU(3)-symmetry, assuming $V_{\{10\}} = V_{\{10^*\}}$. In the ESC models the $V_{10} \approx V_{10^*}$, see [3], and the singlet-triplet transitions are small. So, we conclude that R-conjugation is an approximate symmetry in the ESC models, and is broken mainly "kinematically" similarly as SU(3).

Assuming approximate R-conjugation symmetry, in the ESC16* model we could set $C_{10} = C_{10^*}, S_{10} = S_{10^*}$, and $T_{10} = T_{10^*}$. Doing so leads to an equally good fit to the NN$\oplus$YN data, and is a useful limit on the number of free parameters.

We follow the Thompson approach [34–37] and expressions for the potential in momentum space can be found in Ref. [23]. Since the nucleons have strangeness $S = 0$, the hyperons $S = -1$, and the cascades $S = -2$, the possible baryon-baryon interaction channels can be classified according to their total strangeness, ranging from $S = 0$ for NN to $S = -4$ for $\Xi\Xi$. Apart from the wealth of accurate NN scattering data for the total strangeness $S = 0$ sector, there are only a few, and not very accurate, YN scattering data for the $S = -1$ sector, while there are no data at all for the $S < -1$ sectors. We therefore believe that at this stage it is not yet worthwhile to explicitly account for the small mass differences between the specific charge states of the baryons and mesons; i.e., we use average masses, isospin is a good quantum number, and the potentials are calculated on the isospin basis. The possible channels on the isospin basis are given in (2.2).

However, the Lippmann-Schwinger or Schrödinger equation is solved for the physical particle channels, and so scattering observables are calculated using the proper physical baryon masses. The possible channels on the physical particle basis can be classified according to the total charge Q; these are given in (2.1). The corresponding potentials are obtained from the potential on the isospin basis by making the appropriate isospin rotation. The matrix elements of the isospin rotation matrices are

nothing else but the Clebsch-Gordan coefficients for the two baryon isospins making up the total isospin. (Note that this is the reason why the potential on the particle basis, obtained from applying an isospin rotation to the potential on the isospin basis, will have the correct sign for any coupling constant on a vertex which involves a Σ^+.)

In order to construct the potentials on the isospin basis, we need first the matrix elements of the various OBE exchanges between particular isospin states. Using the iso-multiplets (2.9) and the Hamiltonian (2.10) the isospin factors can be calculated. The results are given in Table III, where we use the pseudoscalar mesons as a specific example. The entries contain the flavor-exchange operator P_f, which is $+1$ for a flavor symmetric and -1 for a flavor anti-symmetric two-baryon state. Since two-baryons states are totally anti-symmetric, one has $P_f = -P_x P_\sigma$. Therefore, the exchange operator P_f has the value $P_f = +1$ for even-L singlet and odd-L triplet partial waves, and $P_f = -1$ for odd-L singlet and even-L triplet partial waves. In order to understand Table III fully, we have given in the following section Sec. III a general treatment of exchange forces. This treatment shows also how to deal with the case where the initial/final state involves identical particles and the final/inition state does not.

Second, we need to evaluate the TME and the MPE exchanges. The method we used for these is the same as for hyperon-nucleon, and is described in [11], Sec. IID.

TABLE III: Isospin factors for the various meson exchanges in the different channels with total strangeness and isospin. P_f is the flavor-exchange operator. Non-exixisting channels are marked by a long-dash.

$S=-3$	$I=1/2$	$I=3/2$
$(\Lambda\Xi\|\eta,\eta'\|\Lambda\Xi)$	1	—
$(\Sigma\Xi\|\eta,\eta'\|\Sigma\Xi)$	1	1
$(\Sigma\Xi\|\pi\|\Sigma\Xi)$	-2	1
$(\Sigma\Xi\|\pi\|\Lambda\Xi)$	$-\sqrt{3}$	—
$(\Lambda\Xi\|K\|\Xi\Lambda)$	P_f	—
$(\Sigma\Xi\|K\|\Xi\Sigma)$	$-P_f$	$2P_f$
$(\Lambda\Xi\|K\|\Xi\Sigma)$	$P_f\sqrt{3}$	—
$S=-4$	$I=0$	$I=1$
$(\Xi\Xi\|\eta,\eta'\|\Xi\Xi)$	$\frac{1}{2}(1-P_f)$	$\frac{1}{2}(1+P_f)$
$(\Xi\Xi\|\pi\|\Xi\Xi)$	$-\frac{3}{2}(1-P_f)$	$\frac{1}{2}(1+P_f)$

TABLE IV: Baryon masses in MeV/c^2.

Baryon		Mass
Nucleon	p	938.2796
	n	939.5731
Hyperon	Λ	1115.60
	Σ^+	1189.37
	Σ^0	1192.46
	Σ^-	1197.436
Cascade	Ξ^0	1314.90
	Ξ^-	1321.32

III. EXCHANGE FORCES

The proper treatment of the flavor-exchange forces is for the $S < -2$-channels more difficult than for the $S = 0, -1$-channels. The extra complication is the occurrence of coupling between channels with identical and non-identical particles.

IV. MULTI-CHANNEL THRESHOLDS S=-3 CHANNELS

As seen from (2.1) the $S = -3$ two-baryon channels consist of two separate coupled-channel systems separated by the charge. The thresholds are due to the baryon mass differences. The used baryon masses are the same as in [1–3], and are given in Table IV. The laboratory momenta, starting from the baryons at the lowest threshold, are as follows [12]:
For $(\Xi^-\Lambda, \Xi^0\Sigma^-, \Xi^-\Sigma^0)$:

$$\begin{aligned} p^{th}_{lab}(\Xi^-\Lambda \to \Xi^0\Sigma^-) &= 680.4? \text{ MeV/c}, \\ p^{th}_{lab}(\Xi^-\Lambda \to \Xi^-\Sigma^0) &= 694.0 \text{ MeV/c}. \end{aligned} \quad (4.1)$$

For $(\Xi^0\Lambda, \Xi^0\Sigma^0, \Xi^-\Sigma^+)$:

$$\begin{aligned} p^{th}_{lab}(\Xi^0\Lambda \to \Xi^0\Sigma^0) &= 690.0 \text{ MeV/c}, \\ p^{th}_{lab}(\Xi^0\Lambda \to \Xi^-\Sigma^+) &= 706.5 \text{ MeV/c}. \end{aligned} \quad (4.2)$$

The meson masses are the same as in [1–3], as well as the cut-off masses. The threshold differences lead to effective masses for the meson with non-zero strangeness, see [3, 12, 38] for details and references. For S=-3 channels these masses areR for the pseudoscalar meson $m_K = 453.4$ MeV, and the vector meson $m_{K^*} = 869.1$ MeV, These effects are not included for the scalar and axial mesons.

A further subdivision is according to the total isospin. The different thresholds have been discussed in detail in [12], and we show them here in Fig. 1 for the purpose of general orientation. Their presence turns the Lippmann-Schwinger and Schrödinger equation into a coupled-channel matrix equation, where the different channels open up at different energies. In general one has a combination of 'open' and 'closed' channels. For a discussion of the solution of such a mixed system, we refer to [38].

V. PARAMETERS

A complete set of meson coupling constants for ESC16 and ESC16⋆ are given in Appendix B, Tables VI, and VII, respectively. The corresponding meson-pair couplings are given in Appendix C, Tables VIII, and IX, respectively.

VI. RESULTS

Comparison of the parameter matrices for the different models in this paper show that the differences are not large, and we found that the results for the S=-3,-4 are not significantly different. Therefore, we restrict for the detailed results to ESC16 model.
The main purpose of this paper is to present the properties of the ESC16, and ESC16⋆ potentials for the $S = -3, 4$ sectors. We will show the detailed results for ESC16, which are sufficient to represent the possible kind of results. The free parameters in each model are fitted to the NN and YN scattering data for the $S = 0$ and $S = -1$ sectors, respectively. Given the expressions for the coupling constants in terms of the octet and singlet parameters and their values for the six different models as presented in Ref. [22], it is straightforward to evaluate all possible baryon-baryon-meson coupling constants needed for the $S \leq -2$ potentials.

In the following we will present the model predictions for scattering lengths, bound states, and cross sections.

A. Effective-range parameters

ESC08c:

For ESC08c the S=-4 low-energy parameters are

$$\begin{aligned} a_{\Xi\Xi}(^1S_0) &= -1.11\ [fm], \quad r_{\Xi\Xi}(^1S_0) = 6.27\ [fm], \\ a_{\Xi\Xi}(^3S_1) &= +0.54\ [fm], \quad r_{\Xi\Xi}(^3S_1) = 2.28\ [fm]. \end{aligned}$$

For ESC08c the (S=-3,I=1/2) low-energy parameters are

$$\begin{aligned} a_{\Lambda\Xi^0}(^1S_0) &= -5.865\ [fm], \ r_{\Lambda\Xi^0}(^1S_0) = 2.621\ [fm], \\ a_{\Lambda\Xi^0}(^3S_1) &= -3.307\ [fm], \ r_{\Lambda\Xi^0}(^3S_1) = 2.496\ [fm]. \end{aligned}$$

Around the $\Sigma\Xi^0$-threshold for I=1/2 states

$$\begin{aligned} \Sigma\Xi^0(^1S_0)\ :\ A^{-1} &= \begin{pmatrix} 22.656 & 1.317 \\ 1.317 & -0.631 \end{pmatrix}, \\ R &= \begin{pmatrix} 140.978 & 15.458 \\ 15.458 & 1.441 \end{pmatrix}, \\ \Sigma\Xi^0(^3S_1)\ :\ A^{-1} &= \begin{pmatrix} 11.824 & 31.046 & -0.092 \\ 31.046 & 47.621 & 3.780 \\ -0.092 & 3.780 & -0.164 \end{pmatrix}, \\ R &= \begin{pmatrix} 33.555 & 96.183 & -1.234 \\ 96.183 & -216.390 & 21.724 \\ -1,234 & 21.724 & 0.376 \end{pmatrix}, \end{aligned}$$

ESC16:

For ESC16 the S=-4 low-energy parameters are

$$\begin{aligned} a^C_{\Xi\Xi}(^1S_0) &= -1.81\ [fm], \quad r^C_{\Xi\Xi}(^1S_0) = 3.89\ [fm], \\ a_{\Xi\Xi}(^1S_0) &= -1.90\ [fm], \quad r_{\Xi\Xi}(^1S_0) = 4.28\ [fm], \\ a_{\Xi\Xi}(^3S_1) &= +0.52\ [fm], \quad r_{\Xi\Xi}(^3S_1) = 2.74\ [fm]. \end{aligned}$$

Around the $\Sigma\Xi^0$-threshold for I=1/2 states

$$\begin{aligned} \Sigma\Xi^0(^1S_0)\ :\ A^{-1} &= \begin{pmatrix} 31.537 & -29.454 \\ -29.454 & 34.928 \end{pmatrix}, \\ R &= \begin{pmatrix} 89.479 & 19.524 \\ 19.524 & -160.211 \end{pmatrix}, \\ \Sigma\Xi^0(^3S_1)\ :\ A^{-1} &= \begin{pmatrix} 1.708 & 2.377 & 0.662 \\ 2.377 & 62.133 & -16.828 \\ 0.662 & -16.828 & 2.377 \end{pmatrix}, \\ R &= \begin{pmatrix} -0.208 & 13.675 & -3.522 \\ 13.675 & -472.466 & 98.143 \\ -3.522 & 98.143 & -15.637 \end{pmatrix}, \end{aligned}$$

ESC16⋆(A):

In III we have introduced in the ESC16 model SU(3)-symmetric central and spin-spin gaussian-contact BB s-channel potentials

$$W_{\mu,c}(r) = A_\mu f_W(r),\ W_{\mu,\sigma}(r) = B_\mu f_W(r) \boldsymbol{\sigma}_1 \cdot \boldsymbol{\sigma}_2,$$

where $f_W(r) = m_W \exp(-m_W^2 r^2)$, $m_W = 300$ MeV. The s-channel coefficients A_μ, B_μ for ESC16⋆(A) are derived from Tables XVIII and XIX in III, and given in Table V. Here, we have chosen to exhibit the s-channel contact-potentials rather than the t,u-channel ones in III. The largest contact-potentials occur in the $\{8_a\}$ and $\{1\}$ irreps.
For ESC16⋆(A) the following effective-range parameters are obtained

$$\begin{aligned} a_{\Xi\Xi}(^1S_0) &= +0.15\ [fm], \quad r_{\Xi\Xi}(^1S_0) = -1.96\ [fm], \\ a_{\Xi\Xi}(^3S_1) &= +0.13\ [fm], \quad r_{\Xi\Xi}(^3S_1) = -2.08\ [fm]. \end{aligned}$$

TABLE V: ESC16*(A): Coupling constants SU(3)-symmetric gaussian potentials.

$\{\mu\}$	$\{27\}$	$\{8_s\}$	$\{1\}$	$\{8_a\}$	$\{10^*\}$	$\{10\}$
$A_{\{\mu\}}$	–0.109	–0.219	–1.568	–3.322	–0.635	–0.635
$B_{\{\mu\}}$	0.156	–0.356	0.459	3.594	0.123	0.123

For ESC1*(A) the (S=-3,I=3/2) low-energy parameters are

$$a_{\Sigma\Xi}(^1S_0) \;=\; -1.41\;[fm],\; r_{\Sigma\Xi}(^1S_0) = 4.29\;[fm],$$
$$a_{\Sigma\Xi}(^3S_1) \;=\; -1.31\;[fm],\; r_{\Sigma\Xi}(^3S_1) = 5.47\;[fm].$$

For ESC16*(A) the (S=-3,I=1/2) low-energy parameters are

$$a_{\Lambda\Xi^0}(^1S_0) \;=\; -1.147\;[fm],\; r_{\Lambda\Xi^0}(^1S_0) = 4.849\;[fm],$$
$$a_{\Lambda\Xi^0}(^3S_1) \;=\; +0.088\;[fm],\; r_{\Lambda\Xi^0}(^3S_1) = 76.227\;[fm].$$

Around the $\Sigma\Xi^0$-threshold for I=1/2 states

$$\Sigma\Xi^0(^1S_0)\;:\; A^{-1} = \begin{pmatrix} 6.641 & 2.230 \\ 2.230 & -1.110 \end{pmatrix},$$
$$R \;= \begin{pmatrix} -18.459 & 10.465 \\ 10.465 & 2.826 \end{pmatrix},$$
$$\Sigma\Xi^0(^3S_1)\;:\; A^{-1} = \begin{pmatrix} 2.750 & 6.882 & -0.150 \\ 6.882 & -89.577 & 2.952 \\ -0.150 & 2.952 & -0.267 \end{pmatrix},$$
$$R \;= \begin{pmatrix} -0.410 & 17.883 & -2.294 \\ 17.883 & -312.978 & 45.798 \\ -2.294 & 45.798 & -3.493 \end{pmatrix},$$

B. Bound states in *S* waves

Comparison ESC08c, ESC16 and ESC16*(A):

The scattering lenghts and effective ranges in both models show no sign of a bound state. In particular this is the case for $\Xi\Xi(^1S_0)$, which shows a weaker attraction than in $pp(^1S_0)$. Similarly for $\Xi\Xi(^3S_1)$. The effective range formula for the pole position of a possible bound state in momentum space is

$$\kappa_\pm \;=\; \left(1 \pm \sqrt{1 - 2r/a}\right),\; B_\pm = -\kappa_\pm^2/(2m_{red}),$$

where the momentum is $p_\pm = i\kappa_\pm$. The pole closest to the lowest threshold is given by κ_-, and (usually) κ_+ is outside the region of the approximate validity of the effective-range formula. which for $\Xi\Xi(^1S_0)$ gives $\kappa_- < 0$, meaning an anti-bound state, and κ_+ is too large for the effective range expansion to be valid. In the case of $\Xi\Xi(^3S_1)$ the root is imaginary, and so no bound state. Similar analysis shows that also in the other channels there do not occur bound states.

A discussion of the possible bound-states, using the SU(3) content of the different $S = 0, -1, -2$ channels is given in [22]. In contrast to the NSC97 models, we find no bound states in the ESC08c and ESC16 models with only genuine two-body potentials.

C. Partial Wave Phase BKS-Parameters

For the *BB*-channels below the inelastic threshold we use for the parametrization of the amplitudes the standard nuclear-bar phase shifts [43]. The information on the elastic amplitudes above thresholds is most conveniently given using the BKS-phases [24–26]. For uncoupled partial waves, the elastic *BB* S-matrix element is parametrized as

$$S = \eta e^{2i\delta}\;,\quad \eta = \cos(2\rho)\;. \tag{6.1}$$

For coupled partial waves the elastic *BB*-amplitudes are 2×2-matrices. The BKS S-matrix parametrization, which is of the type-S variety, is given by

$$S = e^{i\delta} e^{i\epsilon} N\; e^{i\epsilon} e^{i\delta}\;, \tag{6.2}$$

where

$$\delta = \begin{pmatrix} \delta_\alpha & 0 \\ 0 & \delta_\beta \end{pmatrix}\;,\quad \epsilon = \begin{pmatrix} 0 & \epsilon \\ \epsilon & 0 \end{pmatrix}\;, \tag{6.3}$$

and N is a real, symmetric matrix parametrize as

$$N = \begin{pmatrix} \eta_{11} & \eta_{12} \\ \eta_{12} & \eta_{22} \end{pmatrix}\;. \tag{6.4}$$

From the various parametrizations of the N-matrix, we choose the Kabir-Kermode parametrization [27] to represent the N-matrix in the figures. Then, the N-matrix is given by the inelasticity parameters (α, β, φ), called ρ-parameters, as follows

$$N = \begin{pmatrix} \cos(2\alpha) & \sin(\varphi + \xi) \\ \sin(\varphi + \xi) & \cos(2\beta) \end{pmatrix}\;, \tag{6.5}$$

where

$$\alpha = \pm\frac{1}{2}\cos^{-1}(\eta_{11})\;\;,\;\; \beta = \pm\frac{1}{2}\cos^{-1}(\eta_{22})\;,$$
$$\varphi = \sin^{-1}(\eta_{12}) - sgn(\eta_{12})\sin^{-1} Q$$
$$\xi = sgn(\eta_{12})\sin^{-1} Q\;. \tag{6.6}$$

Here

$$Q^2 = 1 - |\eta_{11} + \eta_{22}| + \eta_{11}\eta_{22}\;. \tag{6.7}$$

?The $^3S_1$-phase shows that there is a resonance below ?the ΣN-threshold, the so-called analogue of the deuteron. This signals ?the fact that in the $\Sigma\Xi^0(^3S_1, I = 1/2)$-state there is a strong attraction.

In Fig's 2-6 the BKS-phases and coupling parameters (α, β, φ) for ESC16 are shown.

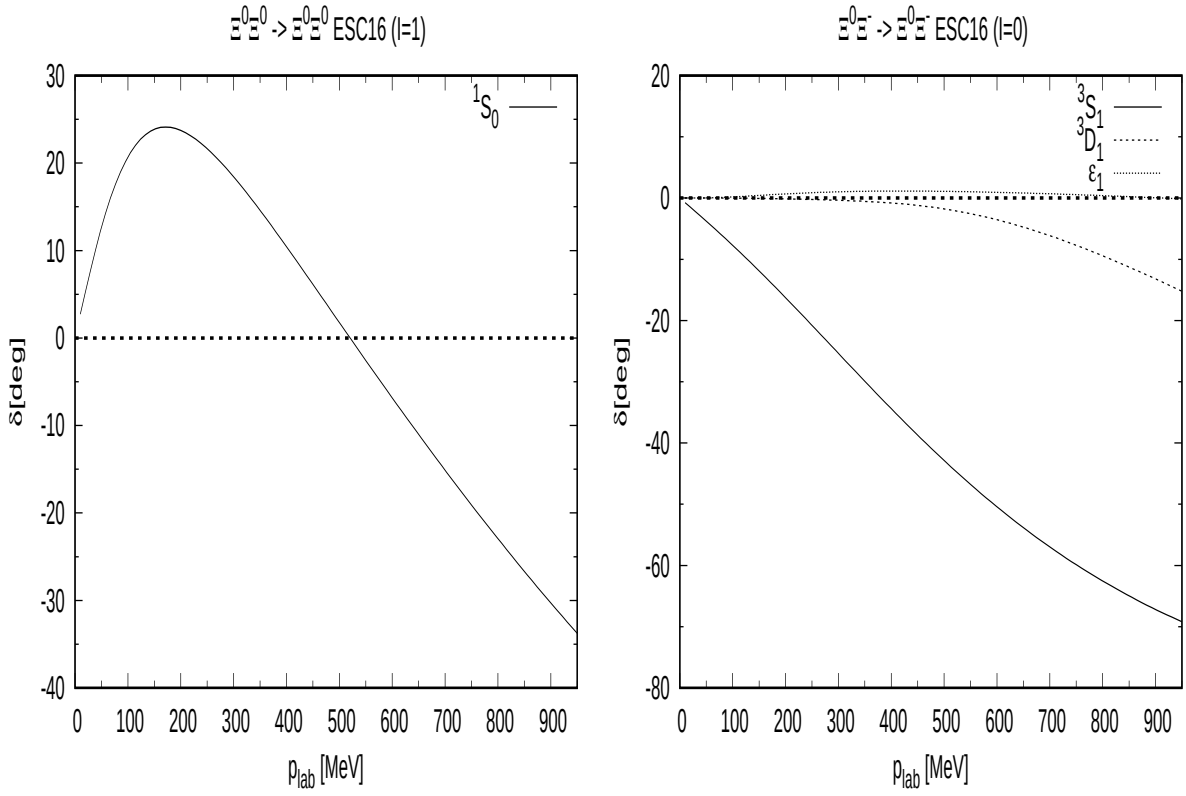

FIG. 2: ESC16 $\Xi^0\Xi^0(^1S_0, I=1)$- and $\Xi^0\Xi^-(^3S_1, I=0)$ phases.

The $\Xi^-\Xi^-, \Xi^0\Xi-, \Xi^0\Xi^0$ nuclear-bar phase shifts for I=1 and I=0 as a function of the momentum and energy are given in the tables in Appendix D for ESC16 and in Appendix E for ESC16*(A). Similarly, for the BKS-parameters $\Lambda\Xi^0, \Lambda\Xi(I=1/2), \Sigma\Xi^0(I=1/2)$, and $\Sigma^+\Xi^0(I=3/2)$. the inelasticity parameters ρ and $\eta_{11}, \eta_{12}, \eta_{22}$, which contains the information to construct the $\delta-$, $\epsilon-$, N- and S-matrix.

Notice that the $^3S_1$-phase shows repulsion, except for very low energies. This means that the the potential has a weak long range attractive tail.

VII. SUMMARY AND CONCLUSION

The ESC08 models potentials presented here are a major step in constructing the baryon-baryon interactions for scattering and hypernuclei in the context of broken SU(3)$_F$ symmetry. The dynamical ingredients are (i) meson-exchange, and (ii) diffractive/multi-gluon-exchange in the form of gaussian Pomeron and Odderon potentials. The potentials for meson-exchange are based on (i) One-boson-exchanges, where the coupling constants at the baryon-baryon-meson vertices are restricted by the broken SU(3) symmetry, (ii) Two-pseudoscalar exchanges, (iii) Meson-Pair exchanges. Each type of meson exchange (pseudoscalar, vector, axial-vector, scalar) contains five free parameters: a singlet coupling constant, an octet coupling constant, the $F/(F+D)$ ratio α, a meson-mixing angle. The potentials are regularized with gaussian cut-off parameters, which provide a few additional free parameters. The SU(3)-breaking enters only via the physical masses, both for the baryons and the mesons. All coupling constants are asuumed to be SU(3)-symmetric, this in contrast to ESC04a,b. Also, in ESC08a,b we have pseudo-vector coupling, i.e. $a_{PV}=1$, for the pseudo-scalar mesons. So, in these respects ESC08a,b are similar to ESC04d. For a description of the differences with ESC04d we refer the reader to the Introduction. The assumption of SU(3) symmetry then allows us to extend these models to the higher strangeness channels (i.e., *YY* and all interactions involving cascades), without the need to introduce additional free parameters. Like the NSC97 models, the ESC08 models are very powerful models of this kind, and the very first realistic ones.

Although we performed truly simultaneous fits to the *NN* and *YN* data, effectively most of these parameters are determined in fitting the rich and accurate *NN* scattering data, while the remaining ones are fixed by fitting

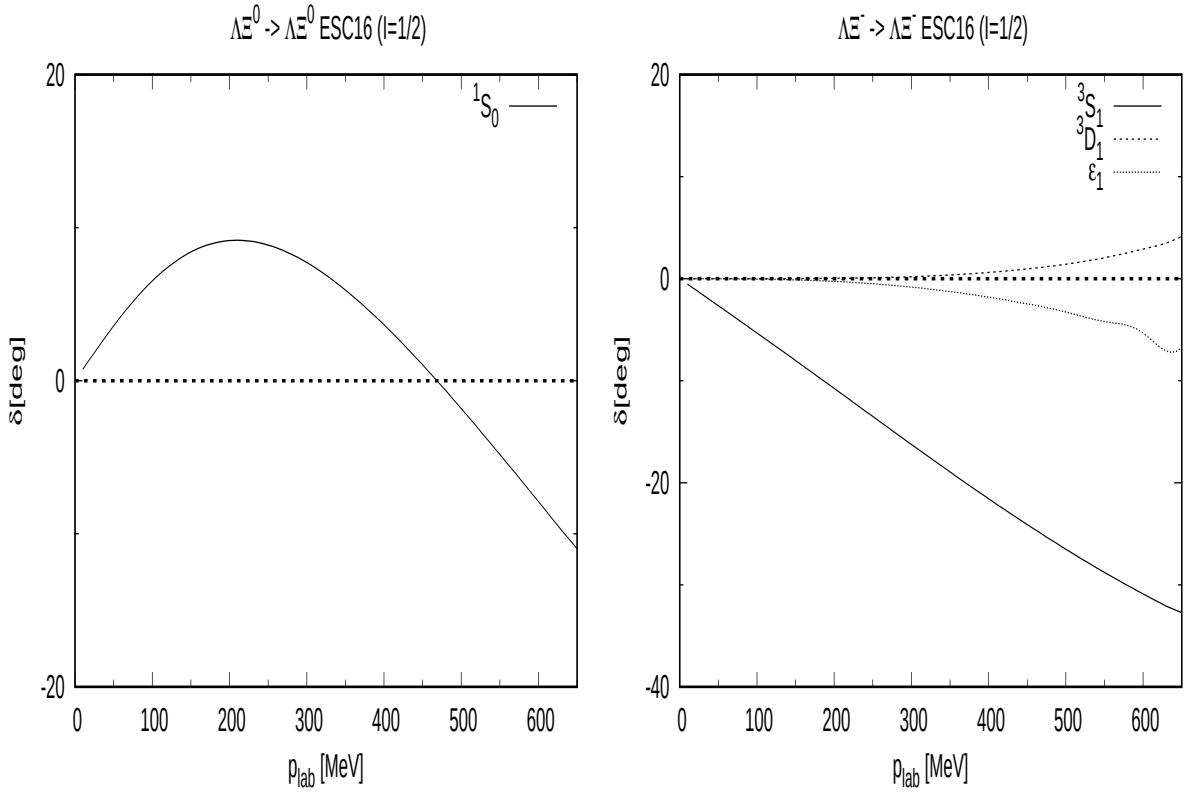

FIG. 3: ESC16 $\Lambda\Xi$ $I = 1/2$ phases.

also the (few) *YN* scattering data. The difference between ESC08a and ESC08b is that in the latter we let the $\Xi N(I = 1,^3 S_1)$-channel to develop a bound-state, i.e. the deuteron D_N=D(Y=0). It occurred that in doing so both the fits to the *NN* and *YN* data improved. In the ESC08b-model we found, for the first time, that the inclusion of the *YN* data plus various other desiderata from hypernuclei did not prohibit a truly excellent *NN*-fit with $\chi^2_{p.d.p.}$1.135. In order to illustrate the basic properties of these potentials, we have presented results for scattering lengths, possible bound states in S-waves, and total cross sections.

We finally mention that these ESC08 potentials also provide an excellent starting point for calculations on multi-strange systems. For that purpose it is necessary that we extend this work to the $S = -3, 4$-systems, i.e. comprising all $\{8\} \otimes \{8\}$ baqryon-baryon states.

Acknowledgments

Th.A.R. would like to thank P.M.M. Maessen and V.G.J. Stoks, for their collaboration in constructing the soft-core $S = -2, -3, -4$ OBE-model.

APPENDIX A: SU(3)-IRREPS AND BARYON-BARYON ISOSPIN-STATES

The BB-irreps are diplayed in Fig. 7 and Fig. 8 showing the two-baryon content, and the hyprcharge Y=N+S of the SU(2)-isospin multiplets.

APPENDIX B: MESON COUPLING CONSTANTS

In Table VI and Table VII we give the MPE-couplings for models ESC16 and ESC16* respectively.

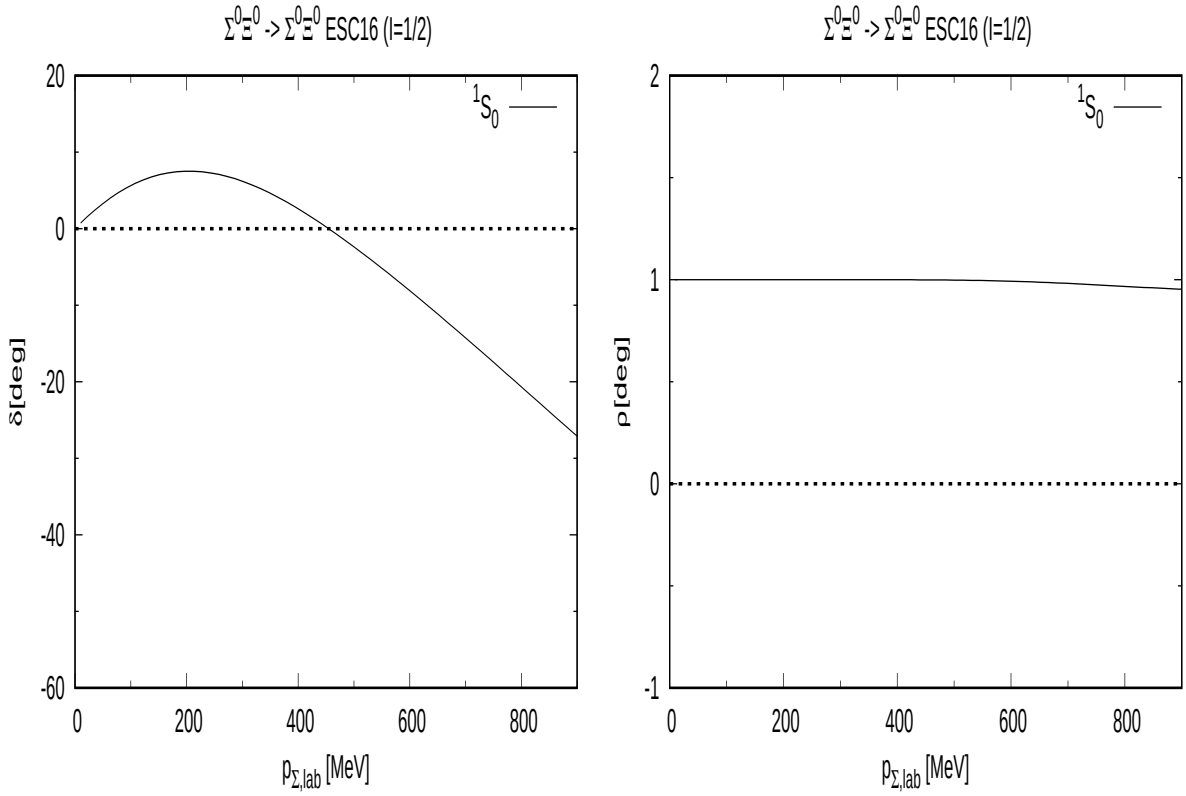

FIG. 4: ESC16 $I = 1/2$ ${}^1S_0(\Sigma^0\Xi^0)$ phases and inelasticities.

APPENDIX C: MESON-PAIR COUPLING CONSTANTS

In Table VIII and Table IX we give the MPE-couplings for model ESC16, and ESC16⋆b respectively.

APPENDIX D: ESC16 BKS-PHASE PARAMETERS

The ESC16 $\Xi^-\Xi^-$ and $\Xi^-\Xi^0$ nuclear-bar phase shifts as a function of energy are given in Tables XI. The $\Lambda\Xi$ BKS phase shifts iand inelasticities are given in Table XII and Table XIII respectively. Table XIV shows the $\Sigma^0\Xi^0$ phase parameters, and Table XV the I=3/2 $\Sigma^+\Xi^0$ phases. Notice that the ${}^3S_1$-phase shows repulsion, except for very low energies. This means that the the potential has a weak long range attractive tail.

APPENDIX E: ESC16⋆(A) BKS-PHASE PARAMETERS

The ESC16⋆(A) $\Xi^0\Xi^0$ and $\Xi^-\Xi^0$ nuclear-bar phase shifts as a function of energy are given in Tables XVI. The $\Lambda\Xi$ BKS phase shifts and inelasticities are given in Table XVII and Table XVIII respectively. Table XIX shows the $\Sigma^0\Xi^0$ phase parameters, and Table XX the I=3/2 $\Sigma^+\Xi^0$ phases.

[1] M.M. Nagels, Th.A. Rijken, and Y. Yamamoto, Phys. Rev. **C 99**, 044002 (2019).
[2] M.M. Nagels, Th.A. Rijken, and Y. Yamamoto, Phys. Rev. **C 99**, 044003 (2019).
[3] M.M. Nagels, Th.A. Rijken, and Y. Yamamoto, Phys. Rev. **C 102**, 054003 (2020).

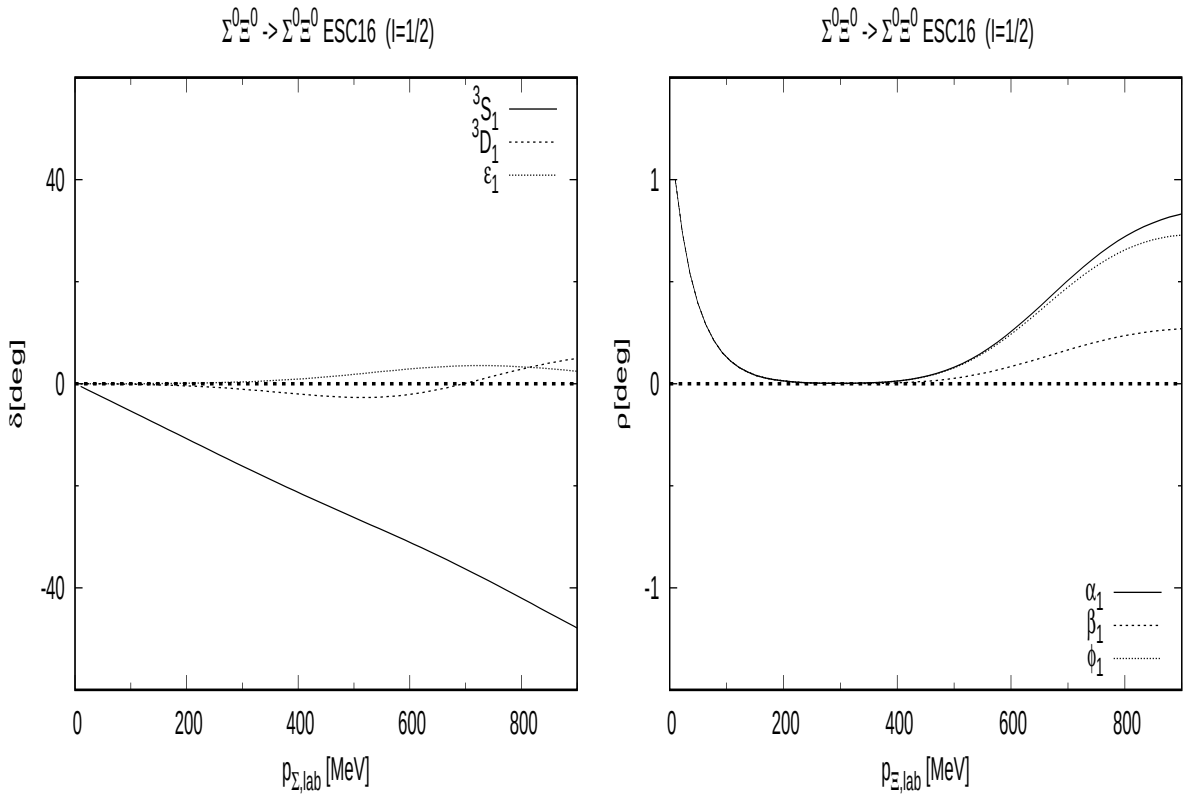

FIG. 5: ESC16 $I = 1/2$ ${}^3C_1(\Sigma^0\Xi^0)$-phases.

[4] k. Nakazawa *et al*, Nucl. Phys. **A 835** (2010) 2-7.
[5] K. Nakazawa *et al*, Progr. Theor. Exp. Phys. **2015**, 033D02.
[6] T. Nagae, Proc. of APPC14, Kuching, Malaaysia, 17-22 November 2019.
[7] M.M. Nagels, Th.A. Rijken, and Y. Yamamoto, *Extended-soft-core Baryon-Baryon Model ESC08c, I. Nucleon-Nucleon Scattering*, [arXiv:nucl-th/1408.4825].
[8] M.M. Nagels, Th.A. Rijken, and Y. Yamamoto, *Extended-soft-core Baryon-Baryon Model ESC08c, II. Hyperon-Nucleon Interactions*, [arXiv:nucl-th/1501.06636],
[9] M.M. Nagels, Th.A. Rijken, and Y. Yamamoto, *Extended-soft-core Baryon-Baryon Model ESC08c, III. Hyperon-Hyperon/Nucleon Interactions*, [arXiv:nucl-th/1504.02634.
[10] Th.A. Rijken, *Extended-soft-core Baryon-Baryon Model. I, Nucleon-Nucleon Interactions*, Phys. Rev. **C73**, 044007 (2006) [arXiv:nucl-th/0603041]
[11] Th.A. Rijken and Y. Yamamoto, *Extended-soft-core Baryon-Baryon Model. II, Hyperon-Nucleon Interactions*, Phys. Rev. **C73**, 044008 (2006) [arXiv:nucl-th/0603042]
[12] V.G.J. Stoks and Th.A. Rijken, Phys. Rev. C **59**, 3009 (1999).
[13] H. Takahashi, et al., Phys. Rev. Lett. **87**, 212502 (2001).
[14] M. Danysz, et al., Nucl. Phys. **49** 121 (1963).
[15] D. J. Prowse, Phys. Rev. Lett. **17** 782 (1966).
[16] See, e.g., B. Shiva Kumar, Nucl. Phys. **A590**, 29c (1995), and references therein.
[17] See, e.g., G. Baym, Nucl. Phys. **A590**, 233c (1995), and references therein.
[18] M. Prakash and J.M. Lattimer, Nucl. Phys. **A639**, 433c (1998), and references therein.
[19] R.L. Jaffe, Phys. Rev. Lett. **38**, 195 (1977); **38**, 617(E) (1977).
[20] L. Micu, Nucl. Phys. **B10**, 521 (1969); A. Le Yaouanc, L. Oliver, O. P'ene, and j.C. Raynal, Phys. Rev. **D8**, 2223 (1973); **9**, 1415 (1974).
[21] N. Isgur and J. Paton, Phys. Rev. **D31**, 2910 (1985); R. Kokoski and N. Isgur, Phys. Rev. **D35**, 907 (1987); T.J. Burns and F.E. Close, Phys. Rev. **D74**, 034003 (2006).
[22] Th.A. Rijken, V.G.J. Stoks, and Y. Yamamoto, Phys. Rev. C **59**, 1 (1999).
[23] P.M.M. Maessen, Th.A. Rijken, and J.J. de Swart, Phys. Rev. C **40**, 2226 (1989).
[24] R.A. Bryan, Phys. Rev. C **24**, 2659 (1981); **30** 305 (1984).
[25] S. Klarsfeld, Phys. Lett. **126b**, 148 (1983).

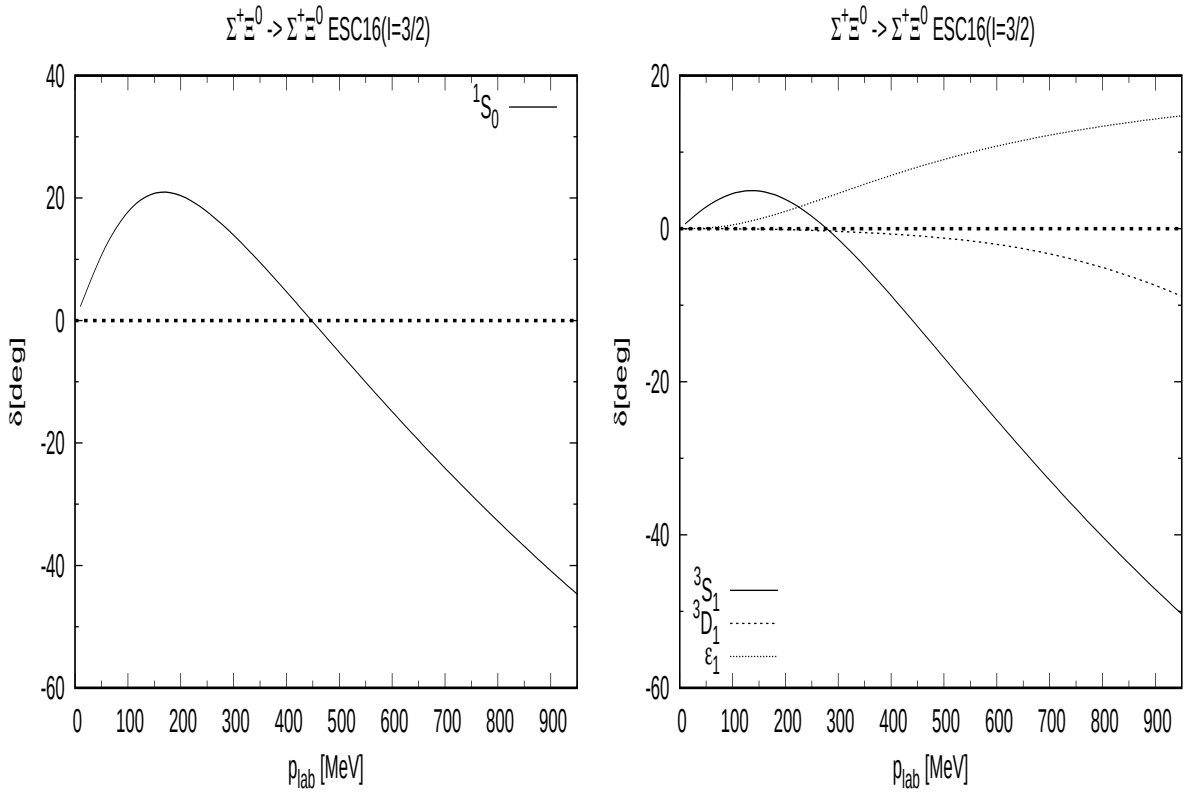

FIG. 6: ESC16 $I = 3/2$ $\Sigma^+\Xi^0$-phases.

[26] D.W.L. Sprung, Phys. Rev. C **32**, 699 (1985).
[27] A. Kabir and M.W. Kermode, J.Phys.G:Nucl.Phys. **13** (1987) 501.
[28] M.M. Nagels, T.A. Rijken, and J.J. de Swart, Ann. Phys. (N.Y.) **79**, 338 (1973).
[29] P.M.M. Maessen, private communication.
[30] J.J. de Swart, Rev. Mod. Phys. **35**, 916 (1963); **37**, 326(E) (1965).
[31] E.U. Condon and G.H. Shortley, *The Theory of Atomic Spectra* (Cambridge University Press, Cambridge, England, 1935).
[32] M. Gell-Mann, California Institute of Technology , Report CTSL–20, 1961 (unpublished).
[33] P.A. Carruthers, 'Introductionto unitary symmetry', John Wiley & Sons Inc., New York , 1966.
[34] R.H. Thompson, Phys. Rev. D **1**, 110 (1970).
[35] Th.A. Rijken, Ann. Phys. (N.Y.) **208**, 253 (1991).
[36] Th.A. Rijken and V.G.J. Stoks, Phys. Rev. C **46**, 73 (1992); **46**, 102 (1992).
[37] Th.A. Rijken and V.G.J. Stoks, Phys. Rev. C **54**, 2851 (1996); **54**, 2869 (1996).
[38] J.J. de Swart, M.M. Nagels, T.A. Rijken, and P.A. Verhoeven, Springer Tracts Mod. Phys. **60**, 138 (1971).
[39] J.J. de Swart and C.K. Iddings, Phys. Rev. **128**, 2810 (1962); *ibid* **130**, 319 (1963).
[40] Y.C. Tang and B.C. Herndon, Phys. Rev. **138**, B637 (1965).
[41] A.R. Bodmer and S. Ali, Phys. Rev. **138**, B644 (1965).
[42] R.H. Dalitz, D.H. Davis, P.H. Fowler, A. Montwill, J. Pniewski, and J.A. Zakrewski, Proc. Roy. Soc. (London) **A426**, 1 (1989).
[43] H.P. Stapp, T. Ypsilantis, and N. Metropolis, Phys. Rev. **105**,302 (1957).
[44] P. Khaustov *et al.*, Phys. Rev. **C 61**, 054603 (2000).
[45] M.M. Nagels, T.A. Rijken, and J.J. deSwart, Phys. Rev. D 15 (1977) 2547.
[46] Y.Yamamoto, T.Motoba, H.Himeno, K.Ikeda and S.Nagata, Prog. Theor. Phys. Suppl. **No.117** (1994), 361.
[47] D.E. Lanskoy, private communication.
[48] M. Beiner, H. Flocard, N.V. Giai, and P. Quentin, Nucl. Phys. **A238**, 29 (1975)
[49] T. Yamada and K. Ikeda, Prog. Theor. Phys. **88**, 139 (1992)
[50] S. Ishikawa, M. Tanifuji, Y. Iseri and Y. Yamamoto, Phys. Rev. **C72**, 027601 (2005).
[51] M. Yamaguchi, K. Tominaga, Y. Yamamoto, and T. Ueda, Prog. Theor. Phys. **105**, 627 (2001)

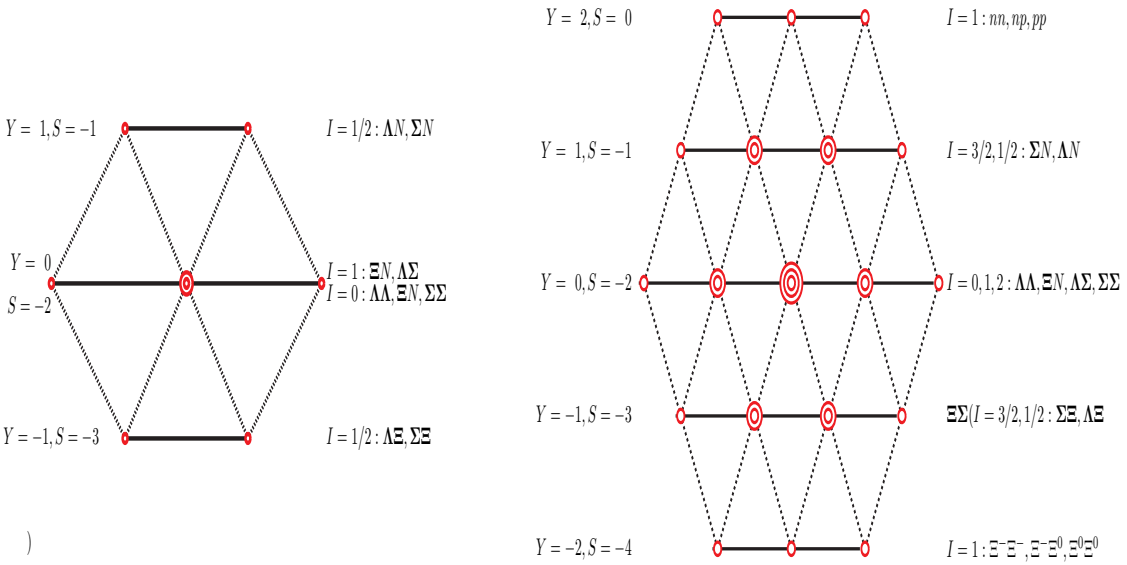

FIG. 7: Baryon-Baryon {8}- and {27}-states.

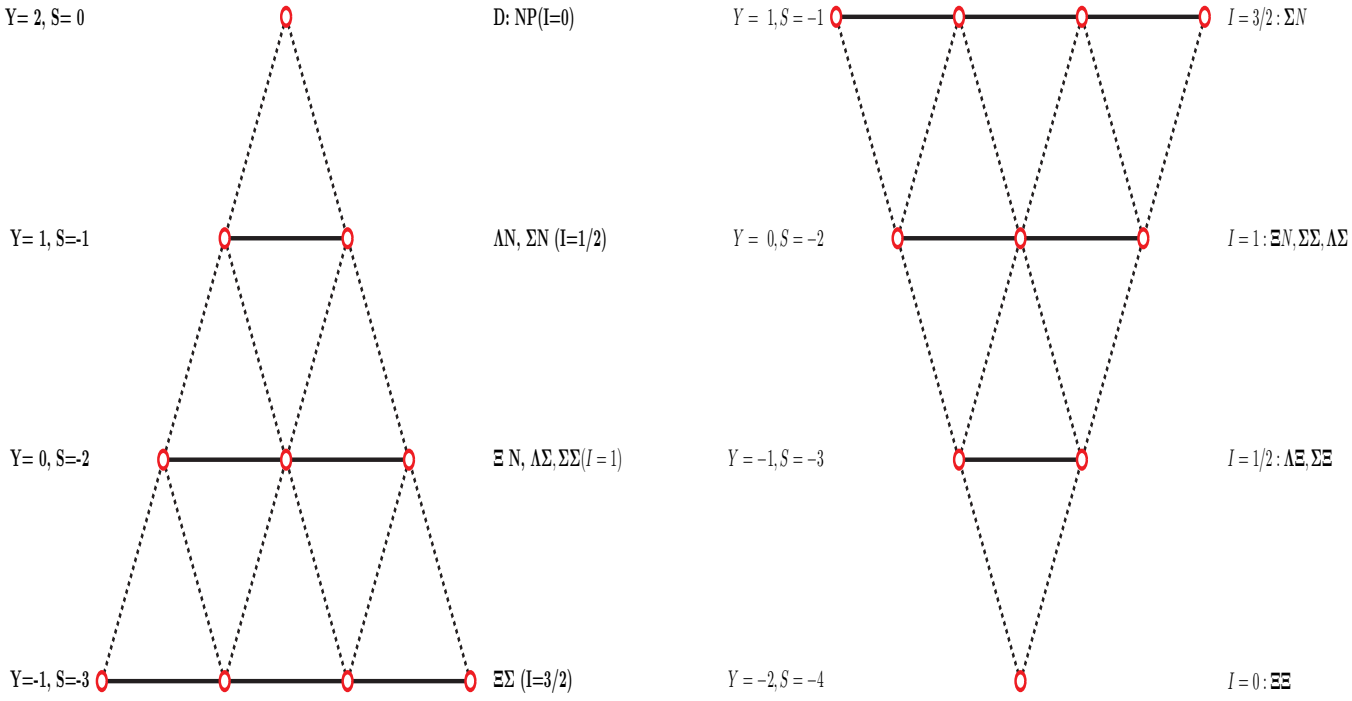

FIG. 8: Baryon-baryon antidecuplet {10*}- and {10}-states.

TABLE VI: Coupling constants for model ESC16, divided by $\sqrt{4\pi}$. M refers to the meson. The coupling constants are listed in the order pseudoscalar, vector (g and f), axial vector A (g and f), scalar, axial vector B, and diffractive.

	M	NNM	$\Sigma\Sigma M$	$\Sigma\Lambda M$	$\Xi\Xi M$	M	ΛNM	$\Lambda\Xi M$	ΣNM	$\Sigma\Xi M$
f	π	0.2684	0.1955	0.1968	–0.0725	K	–0.2681	0.0713	0.0725	–0.2684
g	ρ	0.5793	1.1586	0.0000	0.5793	K^*	–1.0034	1.0034	–0.5793	–0.5793
f		3.7791	3.5185	2.3323	–0.2606		–4.2132	1.8810	0.2606	–3.7791
g	a_1	–0.8172	–0.6260	–0.5822	0.1912	K_{1A}	0.8333	–0.2511	–0.1912	0.8172
f		–1.6521	–1.2656	–1.1770	0.3865		1.6846	–0.5076	–0.3865	1.6521
g	a_0	0.5393	1.0786	0.0000	0.5393	κ	–0.9341	0.9341	–0.5393	–0.5393
f	b_1	–2.2598	–1.8078	–1.5656	0.4520	K_{1B}	2.3484	–0.7828	–0.4520	2.2598
	M	NNM	$\Lambda\Lambda M$	$\Sigma\Sigma M$	$\Xi\Xi M$	M	NNM	$\Lambda\Lambda M$	$\Sigma\Sigma M$	$\Xi\Xi M$
f	η	0.1368	–0.1259	0.2599	–0.1958	η'	0.3181	0.3711	0.2933	0.3852
g	ω	3.1148	2.4820	2.4820	1.8492	ϕ	–1.2384	–2.0171	–2.0171	–2.7958
f		–0.5710	–3.2282	–0.2863	–4.4144		2.8878	–0.3819	3.2380	–1.8416
g	f_1'	–0.7596	–0.1213	–1.0133	0.0710	f_1	0.5147	1.0503	0.3019	1.2117
f		–4.4179	–3.1274	–4.9307	–2.7386		4.4754	5.5582	4.0450	5.8844
g	ε	2.9773	2.3284	2.3284	1.6795	f_0	–1.5766	–2.2485	–2.2485	–2.9205
f	h_1'	–1.2386	0.1171	–1.6905	0.5690	h_1	–0.0830	1.8346	–0.7222	2.4738
g	P	2.7191	2.7191	2,7191	2.7197					
g	O	4.1637	4.1637	4.1637	4.1637					
f		–3.8859	–3.8859	–3.8859	–3.8859					

TABLE VII: Coupling constants for model ESC16*, divided by $\sqrt{4\pi}$. M refers to the meson. The coupling constants are listed in the order pseudoscalar, vector (g and f), axial vector A (g and f), scalar, axial vector B, and diffractive.

	M	NNM	$\Sigma\Sigma M$	$\Sigma\Lambda M$	$\Xi\Xi M$	M	ΛNM	$\Lambda\Xi M$	ΣNM	$\Sigma\Xi M$
f	π	0.2680	0.1978	0.1952	–0.0701	K	–0.2689	0.0737	0.0701	–0.2680
g	ρ	0.5821	1.1641	0.0000	0.5821	K^*	–1.0082	1.0082	–0.5821	–0.5821
f		3.7601	3.8215	2.1355	0.0614		–4.3773	2.2418	–0.0614	–3.7601
g	a_1	–0.8526	–0.6681	–0.5988	0.1845	K_{1A}	0.8780	–0.2792	–0.1845	0.8526
f		–3.1888	–2.4987	–2.2395	0.6902		3.2837	–1.0441	–0.6902	3.1888
g	a_0	0.4905	0.8043	0.1019	0.3139	κ	–0.7575	0.6456	–0.3139	–0.4905
f	b_1	–2.4303	–1.9442	–1.6837	0.4861	K_{1B}	2.5256	–0.8419	–0.4861	2.4303
	M	NNM	$\Lambda\Lambda M$	$\Sigma\Sigma M$	$\Xi\Xi M$	M	NNM	$\Lambda\Lambda M$	$\Sigma\Sigma M$	$\Xi\Xi M$
f	η	0.1394	–0.1243	0.2584	–0.1966	η'	0.3181	0.3712	0.2941	0.3858
g	ω	3.0977	2.4618	2.4618	1.8260	ϕ	–1.2183	–2.0007	–2.0007	–2.7831
f		–0.5473	–3.3080	–0.6144	–4.7218		3.3335	–0.0634	3.2510	–1.8032
g	f_1'	–0.7254	–0.0528	–0.9702	0.1611	f_1	0.4301	0.9945	0.2247	1.1739
f		–4.8976	–2.3822	–5.8134	–1.5824		4.2124	6.3231	3.4440	6.9942
g	ε	3.1268	2.6704	2.7949	2.2762	f_0	–1.5956	–2.1876	–2.0261	–2.6989
f	h_1'	–1.2386	0.2194	–1.7246	0.7054	h_1	–0.1553	1.9069	–0.8428	2.5944
g	P	2.8256	2.8256	2,8256	2.8256					
g	O	4.1637	4.1637	4.1637	4.1637					
f		–3.8859	–3.8859	–3.8859	–3.8859					

TABLE VIII: Pair coupling constants for model ESC16, divided by $\sqrt{4\pi}$. $I(M)$ refers to the isospin of the pair M with quantum-numbers J^{PC}.

Pair	J^{PC}	Type	$I(M)$	NNM	$\Sigma\Sigma M$	$\Sigma\Lambda M$	$\Xi\Xi M$	$I(M)$	ΛNM	$\Lambda\Xi M$	ΣNM	$\Sigma\Xi M$
$\pi\eta$	0^{++}	g	1	–0.6881	–1.3763	0.0000	–0.6881	1/2	1.1919	–1.1919	0.6881	0.6881
			0	–1.1919	0.0000	0.0000	1.1919					
$\pi\pi$	1^{--}	g	1	0.2514	0.5028	0.0000	0.2514	1/2	–0.4354	0.4354	–0.2514	–0.2514
			0	0.4354	0.0000	0.0000	–0.4354					
$\pi\pi$	1^{--}	f	1	–1.7729	–1.4183	–1.2283	0.3546	1/2	1.8425	–0.6142	–0.3546	1.7729
			0	–0.6142	1.2283	–1.2283	1.8425					
$\pi\rho$	1^{++}	g	1	5.6913	4.5530	3.9431	–1.1383	1/2	–5.9147	1.9715	1.1383	–5.6913
			0	1.9715	–3.9431	3.9431	–5.9146					
$\pi\sigma$	1^{++}	g	1	–0.3892	–0.3114	–0.2697	0.0778	1/2	0.4045	–0.1348	–0.0778	0.3892
			0	–0.1348	0.2697	–0.2697	0.4045					
$\pi\omega$	1^{+-}	g	1	–0.3281	–0.2624	–0.2273	0.0656	1/2	0.3409	–0.1136	–0.0656	0.3281
			0	–0.1136	0.2273	–0.2273	0.3409					

TABLE IX: Pair coupling constants for model ESC16*, divided by $\sqrt{4\pi}$. $I(M)$ refers to the isospin of the pair M with quantum-numbers J^{PC}.

Pair	J^{PC}	Type	$I(M)$	NNM	$\Sigma\Sigma M$	$\Sigma\Lambda M$	$\Xi\Xi M$	$I(M)$	ΛNM	$\Lambda\Xi M$	ΣNM	$\Sigma\Xi M$
$\pi\eta$	0^{++}	g	1	–0.2683	–0.5365	0.0000	–0.2683	1/2	0.4646	–0.4646	0.2683	0.2683
			0	–0.4646	0.0000	0.0000	0.4646					
$\pi\pi$	1^{--}	g	1	0.2514	0.4071	0.0553	0.1557	1/2	–0.3802	0.3249	–0.1557	–0.2514
			0	0.3249	–0.05530	0.0553	–0.3802					
$\pi\pi$	1^{--}	f	1	–1.7729	–1.3973	–1.2404	0.3756	1/2	1.8303	–0.5899	–0.3756	1.7729
			0	–0.5899	1.2404	–1.2404	1.8303					
$\pi\rho$	1^{++}	g	1	5.8748	1.7084	5.7973	–4.1665	1/2	–4.3782	–1.4192	4.1665	–5.8748
			0	–1.4192	–5.7973	5.7973	–4.3782					
$\pi\sigma$	1^{++}	g	1	–0.3835	–0.1115	–0.3784	0.2720	1/2	0.2858	0.0926	–0.2720	0.3835
			0	0.0926	0.3784	–0.3784	0.2858					
$\pi\omega$	1^{+-}	g	1	–0.4364	–0.3491	–0.3023	0.0873	1/2	0.4535	–0.1512	–0.0873	0.4364
			0	–0.1512	0.3023	–0.3023	0.4535					

TABLE X: ESC16 nuclear-bar $\Xi^-\Xi^-(I=1,{}^1S_0)$ and $\Xi^0\Xi^-(I=0,{}^3S_1)$ phases in degrees.

p_Λ	10	50	100	200	300	400	500	600
$T_{\rm lab}$	0.038	0.95	3.77	15.05	36.63	59.22	91.94	129.85
$^1S_0$	0.04	7.01	17.27	23.71	19.43	11.69	3.05	-5.60
$^3S_1$	-0.75	-3.77	-7.72	-16.27	-25.36	-34.40	-42.86	-50.43
ϵ_1	0.00	0.03	0.19	0.68	1.02	1.14	1.10	0.94
$^3P_0$	0.00	0.02	0.21	0.96	1.09	-0.53	-3.96	-8.63
$^1P_1$	0.00	0.02	0.24	1.64	3.76	15.21	5.13	3.51
$^3P_1$	-0.00	-0.00	-0.02	0.03	0.06	-0.51	-1.94	-4.11
$^3P_2$	0.00	0.01	0.10	0.68	1.31	1.14	-0.11	-2.20
ϵ_2	-0.00	-0.00	-0.01	-0.07	-0.23	-0.47	-0.76	-1.07
$^3D_1$	-0.00	-0.00	-0.01	-0.13	-0.36	-0.80	-1.77	-3.543
$^1D_2$	0.00	0.00	0.01	0.16	0.74	1.95	3.66	5.49
$^3D_2$	0.00	0.00	0.03	0.31	0.93	1.66	2.16	2.18
$^3D_3$	0.00	0.00	0.00	0.04	0.20	0.40	0.37	-0.12

TABLE XI: ESC16 nuclear-bar $\Xi^-\Xi^0$ phases in degrees.

p_Ξ	50	100	200	300	400	500	600	700	800	900
$T_{\rm lab}$	0.95	3.80	15.12	33.79	59.50	91.86	130.42	174.72	224.24	278.51
$^1S_0$	12.65	20.69	23.73	18.44	10.44	1.77	-6.84	-15.11	-22.94	-30.28
$^3S_1$	-3.77	-7.72	-16.27	-25.36	-34.39	-42.85	-50.42	-56.98	-62.54	-67.19
ϵ_1	0.03	0.19	0.68	1.02	1.14	1.10	0.94	0.70	0.40	0.05
$^3P_0$	0.04	0.25	0.99	0.99	-0.78	-4.32	-9.06	-14.41	-19.95	-25.41
$^1P_1$	0.04	0.31	1.78	3.88	5.23	5.03	3.31	0.45	-3.18	-7.29
$^3P_1$	-0.01	-0.02	0.03	0.03	-0.61	-2.10	-4.30	-6.933	-9.75	-12.57
$^3P_2$	0.02	0.13	0.73	1.32	1.09	-0.23	-2.35	-4.90	-7.61	-10.33
ϵ_2	-0.00	-0.01	-0.08	-0.24	-0.48	-0.77	-1.07	-1.36	-1.60	-1.81
$^3D_1$	-0.00	-0.01	-0.13	-0.36	-0.80	-1.77	-3.54	-6.14	-9.42	-13.19
$^1D_2$	0.00	0.01	0.16	0.74	1.94	3.65	5.48	6.98	7.82	7.86
$^3D_2$	0.00	0.03	0.31	0.93	1.66	2.16	2.18	1.64	0.61	-0.77
$^3D_3$	0.00	0.00	0.04	0.20	0.40	0.37	-0.12	-1.11	-2.50	-4.12
ϵ_3	0.00	0.00	0.04	0.15	0.29	0.40	0.48	0.52	0.53	0.51
$^3F_2$	0.00	0.00	0.01	0.07	0.21	0.42	0.55	0.43	-0.11	-1.16

TABLE XII: I=1/2: ESC16 nuclear-bar $\Lambda\Xi^0$ phases in degrees.

p_Λ	10	50	150	250	350	450	550	650
$T_{\rm lab}$	0.038	0.95	8.53	23.56	45.79	74.88	110.40	151.90
$^1S_0$	0.74	3.58	8.41	8.873	5.93	1.04	-4.82	-10.97
$^3S_1$	-0.53	-2.65	-8.02	-13.50	-18.94	-24.09	-28.78	-32.73
ϵ_1	-0.00	-0.00	-0.12	-0.50	-1.26	-2.47	-4.20	-6.76
$^3P_0$	-0.00	-0.00	-0.06	-0.42	-1.42	-3.20	-5.64	-8.52
$^1P_1$	0.00	0.00	0.09	0.24	0.18	-0.32	-1.34	-2.80
$^3P_1$	-0.00	-0.00	-0.10	-0.47	-1.35	-2.79	-4.70	-6.85
$^3P_2$	0.00	0.00	-0.01	-0.15	-0.64	-1.59	-2.98	-4.68
ϵ_2	-0.00	-0.00	-0.00	-0.01	-0.03	-0.06	-0.08	-0.09
$^3D_1$	0.00	0.00	0.01	0.09	0.36	0.96	2.05	4.15
$^1D_2$	0.00	0.00	0.01	0.10	0.41	1.04	1.99	3.20
$^3D_2$	-0.00	-0.00	-0.00	-0.00	-0.03	-0.14	-0.42	-0.87
$^3D_3$	-0.00	-0.00	-0.00	-0.01	-0.09	-0.35	-0.91	-1.80

TABLE XIII: ESC16 $^1S_0$,$^3S_1$ $-^3D_1(\Lambda\Xi \to \Lambda\Xi, I = 1/2)$ BKS-phase parameters in [degrees] as a function of the laboratory momentum p_Λ in [MeV]. The $\Sigma^0\Xi^0$ and $\Sigma^+\Xi^-$ thresholds are at $p_\Lambda = 689.97$ MeV and $p_\Lambda = 706.47$ MeV respectively.

p_Λ	$\delta(^1S_0)$	$\rho(^1S_0)$	$\delta(^3S_1)$	ϵ_1	$\delta(^3D_1)$	η_{11}	η_{12}	η_{22}
10	0.74	1.00	–0.53	–0.00	0.00	1.00	0.00	1.00
50	3.58	1.00	–2.65	–0.00	0.00	1.00	0.00	1.00
100	6.52	1.00	–5.31	–0.04	0.00	1.00	0.00	1.00
150	8.41	1.00	–8.02	–0.12	0.01	1.00	0.00	1.00
200	9.16	1.00	–10.75	–0.27	0.03	1.00	0.00	1.00
250	8.87	1.00	–13.50	–0.50	0.09	1.00	0.00	1.00
300	7.72	1.00	–16.24	–0.83	0.19	1.00	0.00	1.00
350	5.93	1.00	–18.94	–1.26	0.36	1.00	0.00	1.00
400	3.65	1.00	–21.56	–1.80	0.61	1.00	0.00	1.00
450	1.04	1.00	–24.09	–2.47	0.96	1.00	0.00	1.00
500	-1.82	1.00	–26.51	–3.26	1.43	1.00	0.00	1.00
550	-4.82	1.00	–28.78	–4.20	2.05	1.00	0.00	1.00
600	-7.90	1.00	–30.89	–5.32	2.90	1.00	0.00	1.00
650	-10.97	1.00	–32.73	–6.76	4.15	1.00	0.00	1.00
700	-13.80	0.990	–34.47	1.20	5.99	0.92	0.31	0.91
750	-17.14	0.972	–38.66	3.64	4.65	0.88	0.30	0.84
850	-23.997	0.956	–45.41	5.34	3.07	0.87	0.28	0.81
950	-30.624	0.945	–51.22	6.21	1.93	0.87	0.28	0.73
1050	-36.967	0.936	–56.42	6.69	0.70	0.87	0.28	0.71
1150	-42.966	0.928	–61.15	6.91	–0.70	0.88	0.28	0.68
1250	-41.319	0.921	–65.53	6.93	–2.26	0.89	0.29	0.66
1350	-35.927	0.915	–69.50	6.81	–4.06	0.89	0.29	0.64
1450	-30.988	0.908	–73.07	6.59	–5.96	0.90	0.29	0.64

TABLE XIV: ESC16 ${}^1S_0, {}^3S_1 - {}^3D_1 (\Sigma^0\Xi^0 \to \Sigma^0\Xi^0, I = 1/2)$ BKS-phase parameters in [degrees] as a function of the laboratory momentum p_Σ in [MeV]. The $\Sigma^+\Xi^-$-threshold at $p_\Sigma = 138.15$ MeV.

p_Σ	$\delta({}^1S_0)$	$\rho({}^1S_0)$	$\delta({}^3S_1)$	ϵ_1	$\delta({}^3D_1)$	η_{11}	η_{12}	η_{22}
10	–0.18	1.00	0.44	0.00	0.00	0.99	0.00	1.00
50	–0.85	1.00	2.19	0.01	0.00	0.96	0.00	1.00
100	–1.11	0.99	4.46	0.04	0.01	0.94	0.01	1.00
150	2.38	0.83	8.14	–0.09	0.09	0.87	0.00	1.00
200	–3.65	0.67	7.38	–0.42	0.19	0.78	0.01	1.00
250	–10.02	0.59	6.01	–0.63	0.33	0.75	0.03	0.99
300	–16.30	0.55	4.24	–0.75	0.49	0.73	0.04	0.98
350	–22.32	0.52	2.12	–0.77	0.67	0.72	0.05	0.97
400	–28.05	0.50	–0.30	–0.69	0.86	0.71	0.07	0.96
450	–33.45	0.49	–2.99	–0.51	1.03	0.70	0.08	0.95
500	–38.52	0.48	–5.93	–0.27	1.20	0.69	0.09	0.93
550	–43.27	0.48	–9.07	0.04	1.34	0.68	0.09	0.91
600	–42.29	0.48	–12.37	0.37	1.46	0.68	0.10	0.89
650	–38.16	0.48	–15.81	0.72	1.56	0.67	0.10	0.87
700	–34.30	0.49	–19.32	1.04	1.64	0.67	0.10	0.85
750	–30.72	0.50	–22.85	1.34	1.68	0.67	0.10	0.83
850	–24.23	0.52	–29.86	1.78	1.63	0.67	0.09	0.80
950	–18.55	0.55	–36.59	2.05	1.28	0.68	0.08	0.76
1050	–13.51	0.58	–42.90	2.21	0.52	0.69	0.07	0.74
1150	–9.84	0.61	–48.69	2.30	–0.72	0.70	0.06	0.72
1250	–5.02	0.64	–53.98	2.39	–2.41	0.71	0.06	0.70
1350	–1.31	0.67	–58.93	2.51	–4.32	0.72	0.05	0.70
1450	1.94	0.70	–63.54	2.62	–6.62	0.74	0.04	0.69

TABLE XV: I=3/2: ESC16 nuclear-bar $\Sigma^+\Xi^0$ phases in degrees.

p_{Σ^+}	50	150	250	350	450	550	650	750	850	950
$T_{\rm lab}$	1.05	9.42	25.99	50.43	82.28	121.01	166.03	216.72	272.51	332.83
${}^1S_0$	12.15	22.97	19.53	10.95	1.04	-8.89	-18.41	-27.33	-35.62	-43.27
${}^3S_1$	6.08	11.86	9.42	2.98	-4.90	-13.09	-21.11	-28.73	-35.86	-42.47
ϵ_1	0.09	1.38	3.59	5.99	8.21	10.13	11.75	13.10	14.23	15.16
${}^3P_0$	-0.07	-0.97	-2.63	-5.43	-9.75	-15.24	-21.33	-27.53	-33.52	-39.11
${}^1P_1$	-0.07	-1.32	-4.55	-9.70	-16.21	-23.39	-30.68	-37.72	-44.28	-50.21
${}^3P_1$	0.03	0.41	0.06	-1.69	-4.59	-8.15	-11.96	-15.78	-19.45	-22.90
${}^3P_2$	0.01	0.04	-0.23	-1.31	-3.38	-6.19	-9.37	-12.67	-15.93	-19.08
ϵ_2	0.00	0.07	0.20	0.20	0.06	-0.08	-0.15	-0.10	0.05	0.26
${}^3D_1$	-0.00	-0.04	-0.20	-0.45	-0.81	-1.37	-2.22	-3.39	-5.29	-7.67
${}^1D_2$	-0.00	-0.01	0.25	1.33	3.29	5.65	7.65	8.75	8.73	7.62
${}^3D_2$	0.00	0.17	1.07	3.21	6.63	10.63	14.17	16.54	17.55	17.34
${}^3D_3$	0.00	0.02	0.18	0.62	1.26	1.82	1.99	1.58	0.53	-1.11
ϵ_3	0.00	0.01	0.11	0.32	0.69	1.23	1.90	2.65	3.44	4.27
${}^3G_3$	-0.00	-0.00	-0.01	-0.03	-0.05	-0.03	0.08	0.31	0.72	1.35

TABLE XVI: ESC16*(A) nuclear-bar $\Xi^0\Xi^0$ and $\Xi^-\Xi^0$ phases in degrees.

p_Ξ	50	100	200	300	400	500	600	700	800	900
$T_{\rm lab}$	0.95	3.80	15.12	33.79	59.50	91.86	130.42	174.72	224.24	278.51
$^1S_0$	11.40	18.76	21.45	16.07	8.01	-0.72	-9.36	-17.66	-25.51	-32.86
$^3S_1$	-3.48	-7.15	-15.26	-24.03	-32.81	-40.98	-48.21	-54.35	-59.44	-63.59
ϵ_1	0.03	0.17	0.61	0.88	0.92	0.76	0.48	0.11	-0.35	-0.88
$^3P_0$	0.04	0.25	1.03	1.10	-0.63	-4.15	-8.85	-14.12	-19.50	-24.72
$^1P_1$	0.04	0.31	1.75	3.70	4.72	4.08	1.92	-1.33	-5.28	-9.64
$^3P_1$	-0.00	0.01	0.22	0.46	0.06	-1.30	-3.43	-6.05	-8.893	-11.76
$^3P_2$	0.02	0.15	0.89	1.72	1.72	0.62	-1.29	-3.57	-5.96	-8.30
ϵ_2	-0.00	-0.01	-0.07	-0.23	-0.46	-0.74	-1.04	-1.32	-1.57	-1.78
$^3D_1$	-0.00	-0.01	-0.11	-0.28	-0.62	-1.47	-3.12	-5.63	-8.83	-12.53
$^1D_2$	0.00	0.01	0.17	0.78	2.05	3.83	5.69	7.14	7.89	7.80
$^3D_2$	0.00	0.02	0.30	0.94	1.74	2.36	2.51	2.11	1.23	-0.03
$^3D_3$	0.00	0.00	0.05	0.25	0.53	0.59	0.17	-0.76	-2.10	-3.66
ϵ_3	0.00	0.00	0.04	0.14	0.27	0.37	0.44	0.46	0.45	0.42
$^3F_2$	0.00	0.00	0.01	0.07	0.22	0.45	0.61	0.50	-0.06	-1.14

TABLE XVII: I=1/2: ESC16*(A) nuclear-bar $\Lambda\Xi^0$ phases in degrees.

p_Λ	10	50	150	250	350	450	550	650
$T_{\rm lab}$	0.038	0.95	8.53	23.56	45.79	74.88	110.40	151.90
$^1S_0$	1.61	7.72	17.17	18.01	14.07	8.05	11.30	-5.35
$^3S_1$	-0.13	-0.69	-2.61	-5.69	-9.74	-14.30	-19.06	-23.84
ϵ_1	-0.00	-0.00	-0.12	-0.47	-1.12	-2.02	-3.11	-4.30
$^3P_0$	0.00	0.01	0.16	0.40	0.31	-0.45	-1.91	-3.86
$^1P_1$	0.00	0.01	0.17	0.47	0.47	-0.20	-1.62	-3.53
$^3P_1$	0.00	0.01	0.13	0.38	0.45	0.05	-0.87	-2.10
$^3P_2$	0.00	0.01	0.22	0.72	1.21	1.32	0.93	0.08
ϵ_2	-0.00	-0.00	-0.00	-0.01	-0.03	-0.05	-0.06	-0.05
$^3D_1$	0.00	0.00	0.01	0.14	0.56	1.43	2.83	4.98
$^1D_2$	0.00	0.00	0.02	0.16	0.62	1.54	2.91	4.59
$^3D_2$	0.00	0.00	0.00	0.05	0.17	0.34	0.48	0.54
$^3D_3$	0.00	0.00	0.00	0.03	0.07	0.03	-0.22	-0.77

TABLE XVIII: ESC16*(A) $^1S_0$,$^3S_1-^3D_1(\Lambda\Xi \to \Lambda\Xi, I=1/2)$ BKS-phase parameters in [degrees] as a function of the laboratory momentum p_Λ in [MeV]. The $\Sigma^0\Xi^0$ and $\Sigma^+\Xi^-$ thresholds are at $p_\Lambda = 689.97$ MeV and $p_\Lambda = 706.47$ MeV respectively.

p_Λ	$\delta(^1S_0)$	$\rho(^1S_0)$	$\delta(^3S_1)$	ϵ_1	$\delta(^3D_1)$	η_{11}	η_{12}	η_{22}
10	1.61	1.00	–0.13	–0.00	0.00	1.00	0.00	1.00
50	7.72	1.00	–0.69	–0.00	0.00	1.00	0.00	1.00
100	13.67	1.00	–1.52	–0.04	0.00	1.00	0.00	1.00
150	17.17	1.00	–2.61	–0.12	0.01	1.00	0.00	1.00
200	18.43	1.00	–4.00	–0.26	0.05	1.00	0.00	1.00
250	18.01	1.00	–5.69	–0.47	0.14	1.00	0.00	1.00
300	16.43	1.00	–7.62	–0.76	0.30	1.00	0.00	1.00
350	14.07	1.00	–9.74	–1.12	0.56	1.00	0.00	1.00
400	11.21	1.00	–11.98	–1.54	0.93	1.00	0.00	1.00
450	8.05	1.00	–14.30	–2.02	1.43	1.00	0.00	1.00
500	4.71	1.00	–16.67	–2.55	2.05	1.00	0.00	1.00
550	1.30	1.00	–19.06	–3.11	2.83	1.00	0.00	1.00
600	–2.09	1.00	–21.45	–3.69	3.77	1.00	0.00	1.00
650	–5.35	1.00	–23.84	–4.30	4.98	1.00	0.00	1.00
700	–8.16	0.981	–26.28	0.10	6.36	0.99	0.17	0.97
750	–11.74	0.945	–28.80	0.36	7.01	0.98	0.17	0.91
850	–19.42	0.912	–33.44	0.08	7.95	0.98	0.19	0.89
950	–26.85	0.892	–37.97	–0.18	9.27	0.97	0.22	0.87
1050	–34.01	0.878	–42.44	–0.37	10.20	0.96	0.23	0.85
1150	–40.80	0.872	–46.81	–0.53	10.48	0.96	0.23	0.83
1250	–42.77	0.873	–51.09	–0.69	10.11	0.95	0.23	0.81
1350	–36.83	0.879	–55.17	–0.84	9.08	0.94	0.23	0.79
1450	–31.51	0.888	–58.93	–0.98	7.57	0.94	0.22	0.78

TABLE XIX: ESC16*(A) $^1S_0$,$^3S_1$ $-^3D_1(\Sigma^0\Xi^0 \to \Sigma^0\Xi^0, I = 1/2)$ BKS-phase parameters in [degrees] as a function of the laboratory momentum p_Σ in [MeV]. The $\Sigma^+\Xi^-$-threshold at $p_\Sigma = 138.15$ MeV.

p_Σ	$\delta(^1S_0)$	$\rho(^1S_0)$	$\delta(^3S_1)$	ϵ_1	$\delta(^3D_1)$	η_{11}	η_{12}	η_{22}
10	0.75	1.00	7.96	0.00	0.00	0.99	–0.00	1.00
50	3.86	0.99	36.17	0.00	0.00	0.96	–0.00	1.00
100	9.04	0.98	64.73	0.02	0.02	0.98	–0.01	1.00
150	21.73	0.54	–41.70	–0.03	0.06	0.23	0.05	1.00
200	5.03	0.44	15.37	–1.93	0.23	0.25	0.04	1.00
250	–2.78	0.45	18.87	–2.18	0.41	0.40	0.05	0.99
300	–8.41	0.46	18.07	–2.34	0.67	0.49	0.06	0.99
350	–13.13	0.48	16.00	–2.44	1.01	0.56	0.07	0.98
400	–17.32	0.49	13.32	–2.48	1.43	0.61	0.09	0.97
450	–21.10	0.51	10.27	–2.47	1.92	0.64	0.09	0.96
500	–24.53	0.54	7.00	–2.42	2.48	0.67	0.10	0.94
550	–27.65	0.56	3.58	–2.34	3.09	0.69	0.10	0.93
600	–30.48	0.59	0.07	–2.24	3.74	0.70	0.11	0.91
650	–33.06	0.63	–3.50	–2.15	4.40	0.72	0.10	0.89
700	–35.44	0.66	–7.08	–2.07	5.06	0.72	0.10	0.87
750	–37.59	0.69	–10.65	–2.02	5.66	0.73	0.09	0.85
850	–41.48	0.76	–17.62	–2.02	6.67	0.75	0.07	0.81
950	–44.97	0.82	–24.28	–2.09	7.18	0.76	0.05	0.79
1050	–41.75	0.87	–30.56	–2.18	7.09	0.77	0.03	0.76
1150	–38.59	0.90	–36.40	–2.23	6.32	0.78	0.02	0.75
1250	–35.49	0.93	–41.78	–2.21	4.95	0.79	–0.00	0.74
1350	–32.28	0.95	–46.86	–2.15	3.25	0.80	–0.02	0.74
1450	–29.00	0.96	–51.70	–2.03	1.12	0.81	–0.03	0.74

TABLE XX: I=3/2: ESC16*(A) nuclear-bar $\Sigma^+\Xi^0$ phases in degrees.

p_{Σ^+}	50	150	250	350	450	550	650	750	850	950
$T_{\rm lab}$	1.05	9.42	25.99	50.43	82.28	121.01	166.03	216.72	272.51	332.83
$^1S_0$	10.77	20.54	16.99	8.37	-1.59	-11.58	-21.14	-30.11	-38.44	-46.11
$^3S_1$	8.64	16.67	14.29	7.58	-0.48	-8.72	-16.68	-24.18	-31.17	-37.62
ϵ_1	0.10	1.42	3.59	5.87	9.93	9.66	11.07	12.21	13.14	13.89
$^3P_0$	-0.06	-0.88	-2.38	-5.03	-9.24	-14.62	-20.56	-26.53	-32.18	-37.31
$^1P_1$	-0.07	-1.25	-4.34	-9.38	-15.84	-23.06	-30.46	-37.67	-44.46	-50.68
$^3P_1$	0.03	0.48	0.31	-1.21	-3.92	-7.32	-11.01	-14.72	-18.29	-21.66
$^3P_2$	0.01	0.09	-0.07	-1.06	-3.08	-5.84	-8.98	-12.20	-15.35	-18.35
ϵ_2	0.00	0.07	0.19	0.19	0.06	-0.09	-0.15	-0.10	0.04	0.23
$^3D_1$	-0.00	-0.04	-0.19	-0.41	-0.72	-1.23	-2.03	-3.22	-4.89	-7.08
$^1D_2$	-0.00	-0.01	0.29	1.44	3.51	5.94	7.95	8.99	8.85	7.62
$^3D_2$	0.00	0.17	1.09	3.32	6.90	11.08	14.80	17.30	18.41	18.27
$^3D_3$	0.00	0.02	0.19	0.67	1.34	1.91	2.04	1.58	0.49	-1.20
ϵ_3	0.00	0.01	0.10	0.31	0.68	1.22	1.89	2.64	3.43	4.24
$^3G_3$	-0.00	-0.00	-0.01	-0.03	-0.04	-0.01	0.12	0.37	0.81	1.45